Progress in Additive Manufacturing
https://doi.org/10.1007/s40964-025-01481-y

REVIEW

Additively manufactured smart metallic structures with embedded sensing: a review

Sazedur Rahman[1] · Semih Akin[1] · Jinhan Ren[1] · Peiyuan Zhou[1] · Fotis Kopsaftopoulos[1] · Johnson Samuel[1]

Received: 15 July 2025 / Accepted: 12 December 2025

Abstract

The integration of sensors into metallic structures has gained significant attention, leading to the emergence of "Smart Metallic Structures (SMS)." These structures feature embedded sensors designed for real-time data acquisition of functional signals (e.g., strain, temperature, pressure, humidity) for structural monitoring. Notably, the advent of metal additive manufacturing (AM) technologies has enabled the direct embedding of functional sensors into metallic components, making a transformative step toward fully integrated smart structures. This capability is particularly valuable for critical applications where continuous monitoring is vital to ensure safety, efficiency, durability, and improved performance. Despite rapid progress, there remains a need for a comprehensive review that systematically summarizes sensor-embedding strategies, material–process interactions, performance evaluation methods, and key challenges. This review addresses that gap by synthesizing recent developments in additively manufactured SMS and elucidating how AM technologies are being leveraged to integrate sensing functionalities. The objectives of this work are to: (i) consolidate recent advancements; (ii) provide a nuanced perspective on the current landscape of sensor-embedded SMS; and (iii) identify key research challenges to guide future work and facilitate broader adoption. Unlike prior reviews that primarily focus on either AM techniques or standalone sensor technologies, this work presents a holistic framework linking materials, manufacturing processes, and sensing performance. By mapping current progress and outlining emerging opportunities, this review aims to guide both researchers and industry practitioners toward the development of next-generation intelligent metallic systems.

Keywords Additive manufacturing · Smart metallic structures (SMS) · Embedded sensor · Structural health monitoring (SHM)

Abbreviations

AFSD	Additive friction stir deposition
AI	Artificial intelligence
AM	Additive manufacturing
CNC	Computer numerical control
CSAM	Cold spray additive manufacturing
DED	Directed energy deposition
L-DED	Laser-directed energy deposition
DMLS	Direct metal laser sintering
EBM	Electron beam melting
EDM	Electron discharge machining
EMI	Electromagnetic interference
FBG	Fiber Bragg grating
FEA	Finite element analysis
LPBF	Laser powder bed fusion
IC	Integrated circuit
MAM	Metal additive manufacturing
MMAM	Multi-material additive manufacturing

✉ Semih Akin
akins@rpi.edu

Sazedur Rahman
rahmas5@rpi.edu

Jinhan Ren
renj2@rpi.edu

Peiyuan Zhou
zhoup2@rpi.edu

Fotis Kopsaftopoulos
kopsaf@rpi.edu

Johnson Samuel
SAMUEJ2@rpi.edu

[1] Department of Mechanical, Aerospace, and Nuclear Engineering, Rensselaer Polytechnic Institute, Troy, NY 12180, USA

Published online: 20 January 2026

ML	Machine learning
PCB	Printed circuit board
PBF	Powder bed fusion
PVDF	Polyvinylidene fluoride
PZT	Piezoelectric
RFID	Radio frequency identification
RTD	Resistance temperature detector
SAW	Surface acoustic wave
SG	Strain gauge
SHM	Structural health monitoring
SLM	Selective laser melting
SMA	Shape memory alloy
SMS	Smart metallic structures
SMT	Surface mount technology
SR-XRD	Synchrotron radiation X-ray diffraction
TC	Thermocouple
TCR	Transformational challenge reactor
UAM	Ultrasonic additive manufacturing
WAAM	Wire arc additive manufacturing

1 Introduction

Smart structures can be broadly defined as structural components integrated with sensors capable of continuously monitoring and assessing structural integrity, as well as environmental and operating conditions. Such smart structural systems allow for real-time data collection and analysis, improved safety, and optimized performance across various applications, while potentially enabling predictive maintenance schemes. By combining advanced materials, sensor technologies, and data analytics, smart structures can respond to changing conditions, self-diagnose potential issues, and even adapt to their environment, making them essential for future innovations in several industries, including aerospace [1], defense [2], automotive [3, 4], civil engineering [5], energy sector [6], robotic [7], biomedical [8], and beyond.

In recent decades, embedding sensors into polymers and composites has gained significant attention for fabricating smart structures, owing to their lightweight, customizable, and scalable properties [9, 10]. These efforts have driven remarkable advancements in both smart structures and structural health monitoring (SHM) [11–15]. More recently, the integration and embedding of sensors into metallic structures has attracted growing interest, leading to the development of "Smart Metallic Structures (SMS)" [16–22]. Metallic structures, known for their strength, durability, and widespread use in demanding conditions and strategic industries [23], are ideal candidates for sensor integration. Embedding sensors directly into metal parts enables advanced monitoring capabilities (e.g., strain, temperature, pressure, humidity) and facilitates the early detection of wear, fatigue, or failure. These features allow the diagnosis of structural damage and defects, enable predictive maintenance, and minimize downtime in critical applications without compromising the structural integrity, while providing advanced SHM capabilities under varying and potentially harsh environmental and operating conditions [24].

Advancements in additive manufacturing (AM) and SHM are driving the integration of sensors into metallic structures [25]. The increasing number of publications in these areas, as shown in Fig. 1a, highlights the dynamic and synergistic growth of research in AM and SHM. To further contextualize this trend, the figure also incorporates publication data related to "smart structure" and "embedded sensor," demonstrating the growing convergence of these research domains and underscoring their organic development and relevance

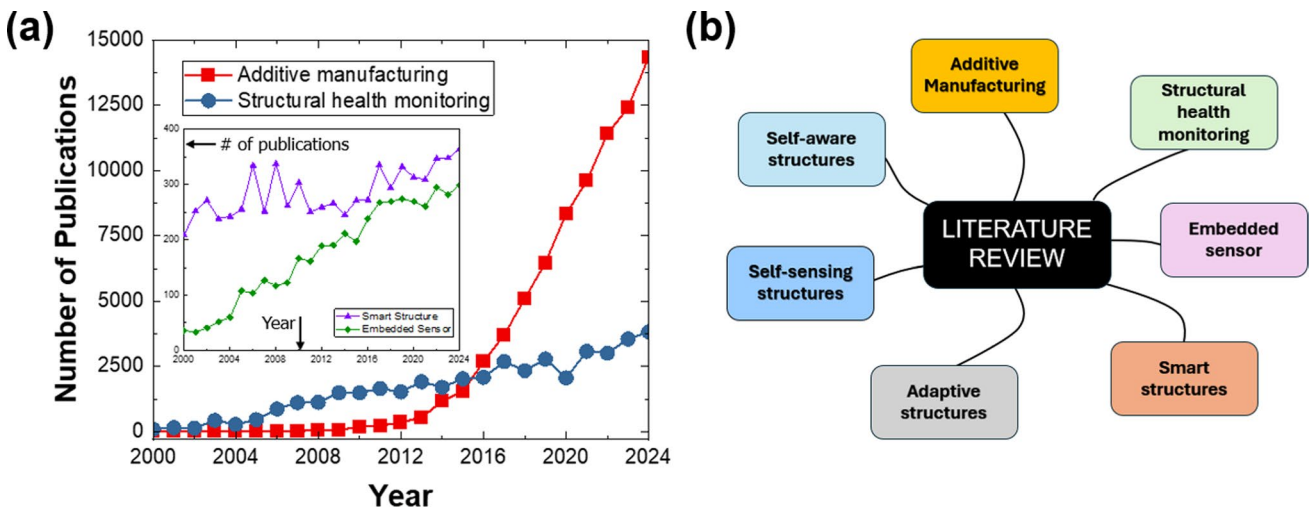

Fig. 1 **a** Growth in peer-reviewed publications related to fields of AM, SHM, Smart structure, and Embedded sensors [Note: data are the number of publications per year as per Scopus keyword search in October 2025]; **b** Keywords used in literature search

to the present review. Notably, Metal Additive Manufacturing (MAM) technologies, with their precision and flexibility [26], enable the direct embedding of sensors into intricate geometries for advanced SHM that would be challenging to achieve through traditional manufacturing processes. This capability facilitates the creation of highly customized, sensor-rich smart metal components that significantly enhance real-time structural monitoring in demanding environments. In this context, the US Defense Advanced Research Projects Agency (DARPA) launched the "*Structural Evaluation through Non-contact Sensor Embedding (SENSE)"* initiative in 2023 [27], aimed at encouraging the development of innovative methods for embedding sensors directly within metallic structures during the AM process. This initiative focuses on advancing structural monitoring for critical metal components used in strategic applications, where real-time performance data and early detection of potential failures are essential for maintaining safety and operational efficiency. Collectively, these advancements in AM, SHM, and sensor integration represent a transformative leap in additively manufactured metal parts.

Despite these advancements and notable trends in the field, there remains a noticeable lack of a review article that consolidates and promotes this emerging subject within AM literature. While several existing reviews have provided valuable insight into sensor-embedded 3-D printed parts [28, 29], a broad synthesis encompassing the full spectrum of additively manufactured SMS with embedded sensing capabilities for SHM has yet to be reported. As such, this review aims to fill that gap by offering a holistic overview of current approaches, technologies, and applications at the intersection of MAM, embedded sensing, and structural monitoring. By discussing the latest research, this work provides the state-of-the-art in AM of SMS, identifies key gaps in the existing knowledge, and proposes potential avenues for future research. The objective of this review is to synthesize recent advancements while offering a nuanced perspective on the current landscape of SMS. By providing a comprehensive evaluation of the current literature, this work seeks to identify future research directions that will facilitate the broader adoption of SMS in industrial applications.

To ensure a comprehensive and systematic assessment, relevant publications were searched and extracted from databases (i.e., Scopus, Web of Science, IEEE Xplore) covering the period 2003–2025. The keywords used in the literature search are illustrated in Fig. 1b. Studies focusing on sensor integration in metallic AM were included, while non-peer-reviewed or irrelevant works (non-metallic AM) were excluded from the analysis. After title, abstract, and full-text screening, eligible articles were categorized and synthesized based on their contributions to sensor selection, fabrication methods, embedding strategies, and performance evaluation.

The study begins with a discussion on AM of SMS (Sect. 2). It first introduces the sensor selection criteria for integration into metallic structures, covering material compatibility, operational requirements, and functional considerations (Sect. 2.1). Subsequently, Sect. 2.2 focuses on the AM techniques used for SMS fabrication, providing a detailed overview of recent advancements along with a comparative analysis of their advantages and limitations. Section 3 presents a comprehensive, step-by-step examination of the sensor embedding processes into AM-built parts, outlining critical stages involved. Section 4 explores the technological benefits and existing challenges of SMS within the context of AM, emphasizing both potential opportunities and barriers to broader adoption. Finally, Sect. 5 outlines the conclusion and sheds light on promising future trends in the field.

2 AM of smart metallic structures

The fabrication of SMS via AM methods is influenced by a multitude of interconnected factors that affect both the manufacturing process and the integrity of the embedded sensors. Figure 2 presents these factors in an Ishikawa (fishbone) diagram. The principal factors influencing the AM of SMS involve: AM process parameters, feedstock material characteristics, embedded sensor specifications, sensor-material interface compatibility, process control variables, thermal protection (packaging) strategies, post-processing techniques, and environmental considerations.

These factors, along with the associated sub-factors, collectively influence the AM of SMS and must be carefully balanced to ensure the structural integrity and functional reliability of the SMS. A holistic understanding of these factors is essential for optimizing the AM process and enhancing the long-term durability and accuracy of the embedded sensors in metal components.

The typical AM methodology employed in the fabrication of SMS is outlined in Fig. 3a–b**,** providing a comprehensive view of the overall SMS fabrication workflow, as summarized below:

i. *Sensor selection and characterization:* Define sensing requirements, evaluate sensor compatibility with the AM process, and identify the appropriate sensor or sensor arrays to be integrated into the SMS.
ii. *AM process selection:* Choose the most suitable MAM process based on the material requirement, design complexity, and compatibility with the selected sensors.

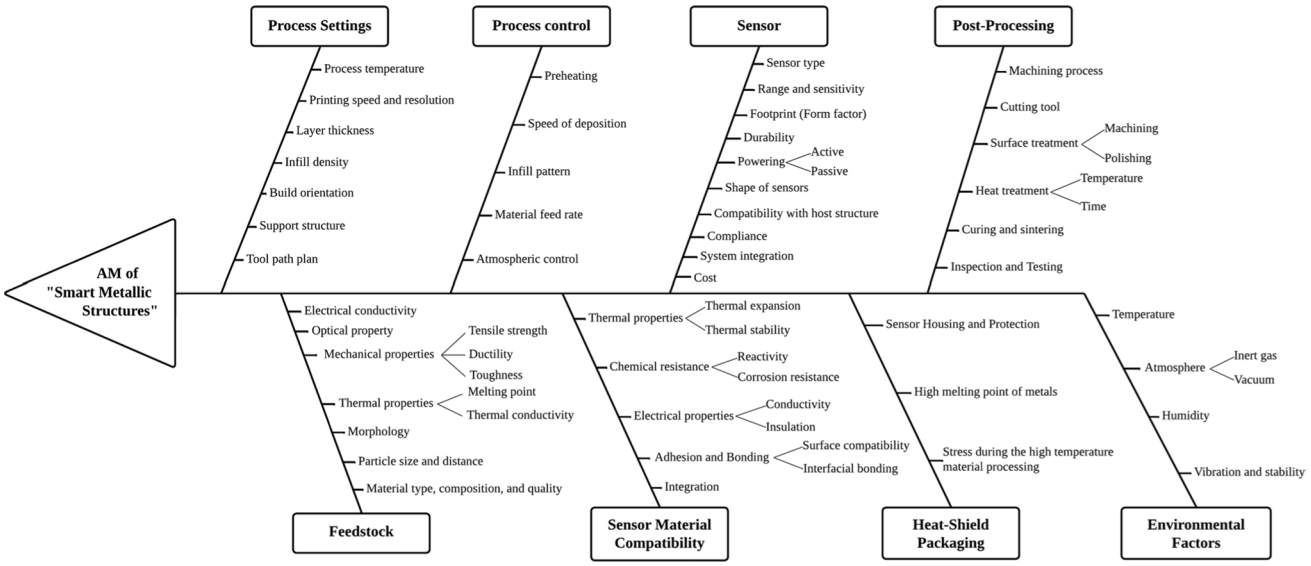

Fig. 2 The key factors influencing AM of SMS

iii. *Host metal fabrication:* Construct the host metal (i.e., bottom layer) using the AM process, as it serves as the foundation for integrating a sensor or overlying material.
iv. *Sensor embedding (integration):* Pause the AM process to embed the sensor into a pre-designed cavity within the host metal. For specific sensors, such as strain gauges or thin-film temperature sensors, a dedicated adhesive film is applied as the sensor bonding layer to ensure accurate data transmission and maintain signal fidelity.
v. *Heat-shield application:* Apply a heat-shield layer or coating (typically made of refractory materials like ceramics) to protect the sensor arrays from high process temperatures and preserve their mechanical and structural integrity during subsequent stages. This step effectively packages the sensor for subsequent manufacturing processes (see Fig. 3c).
vi. *Metal restoration layer:* Apply a metal restoration layer over the sensor to address challenges posed by material inhomogeneity when continuing the AM process on non-metallic materials like ceramics. This step also provides additional thermal protection for sensor arrays.
vii. *Resuming AM process*: Resume the AM process to complete the fabrication of the pre-designed SMS.
viii. *Post-machining*: Apply post-machining to achieve near-net-shape SMS.
ix. *Verify sensor data:* Evaluate the performance and accuracy of the embedded sensors by comparing the recorded data with known reference values (ground truth) under controlled conditions.

The outlined sequential steps have established solid groundwork for the fabrication of SMS using MAM techniques across diverse fields. In particular, the convergence of AM technologies, advancements in material science, and multifunctional sensor integration has driven the development of SMS with embedded intelligence and adaptive functionalities. Over recent decades, these innovations have enabled the realization of SMS with enhanced functionalities across diverse applications. Table 1 provides a summary of the recent progress in additively manufactured SMS, highlighting key areas of focus and outcomes.

2.1 Sensor selection for SMS

The selection of sensors for SMS depends on both the specific properties of the structure being monitored and the requirements of the applications. Sensors used in structural monitoring can be categorized into three primary measurement groups: (i) kinematical (displacement, velocity, acceleration); (ii) mechanical (force, deformation, stress); and (iii) environmental (temperature) [53]. While many sensors are utilized for structural monitoring, strain and acceleration sensors integrated with temperature sensors are generally regarded as the most critical for effective monitoring. Consequently, an increasing amount of research has focused on SMS with embedded strain and temperature sensors. Table 2 lists the primary types of sensors used in SMS, including temperature, strain, vibration, and distance sensors. The following subsections provide an overview of these sensor types, highlighting their key characteristics for SMS.

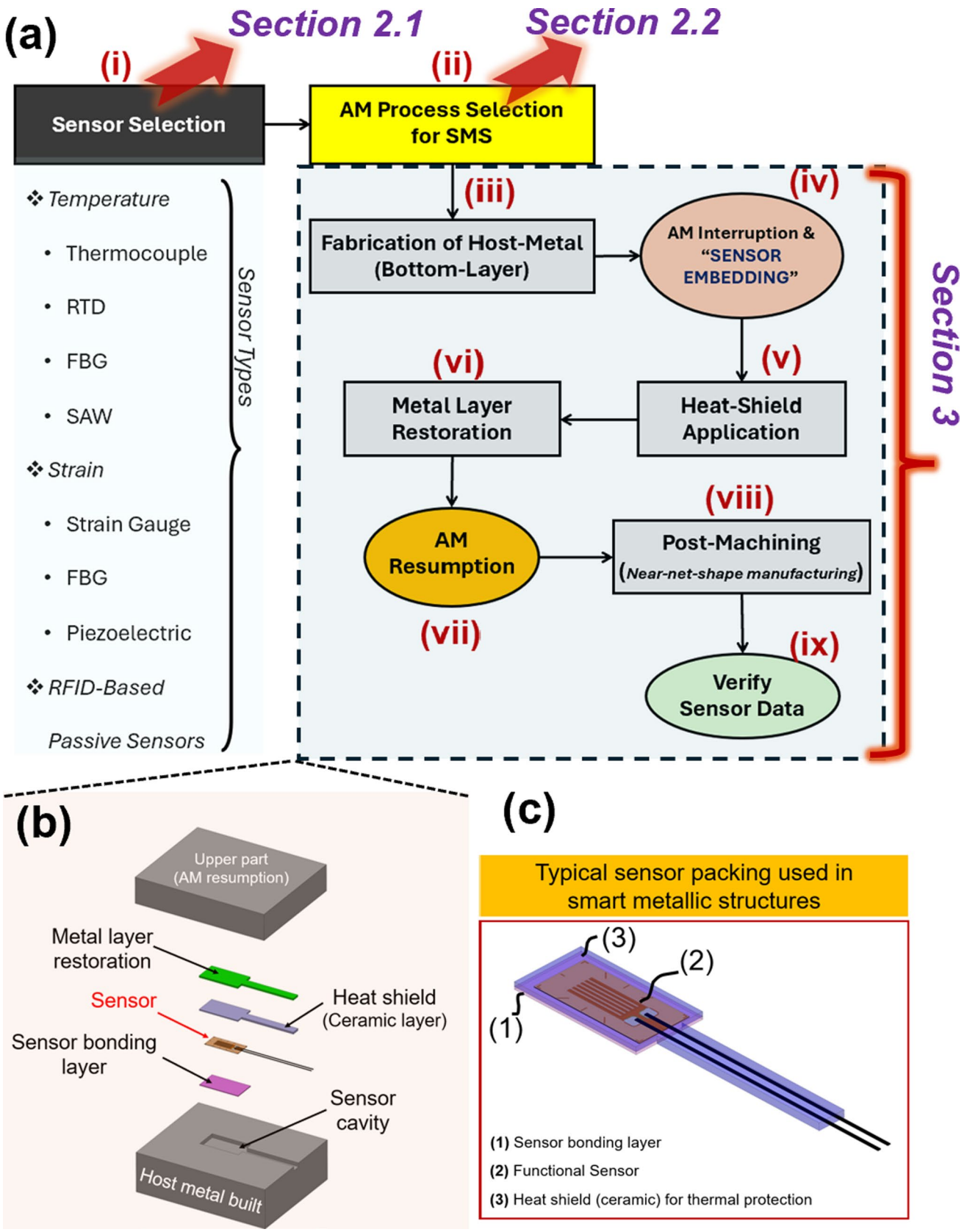

Fig. 3 **a** Process steps for the fabrication of SMS; The schematic of **b** the typical SMS framework; **c** Typical sensor packaging strategy for SMS

Table 1 Summary of recent progress in additively manufactured smart metallic structures

AM method	Year	References	Feedstock material	Sensor	Smart metallic structure (SMS)	Focus	Outcome
LPBF	2025	Freitas Rodrigues et al. [30]	AlSi10Mg	NiTi wire (superelastic SMA strain sensor)	Self-sensing metallic structure	Demonstrated integration of superelastic NiTi strain sensor into AlSi10Mg and studied phase transformation and stress behavior through SR-XRD and FEA	Verified reversible phase transformation and stable resistivity response up to 2.5% strain
	2024	Wang et al. [16]	Ti-6Al-4 V	FBG temperature sensor	ML-assisted sensor-embedded part	Leverage a machine-learning-enhanced FBG temperature sensor to capture real-time data with precision	FBG sensor captured the thermal profile during the LPBF, with a peak temperature of 450 °C
	2024	Šakalys et al. [17]	Stainless steel (316L)	SAW temperature sensor	Smart injection molding tool	Stop-and-go approach to embed a wireless temperature sensor	A smart AM part equipped with a functional wireless sensor, capable of real-time process monitoring
	2024	Ahmed et al. [18]	Inconel 718	FBG strain sensor	Sensor-embedded metal part	3-D integration of sensors into metal components	Embedded sensor performance is hindered by AM process issues, such as poor surface quality and staircasing
	2022	Binder, Machnik, et al. [31]	Inconel 718	Strain gauge	Smart vibration detector	Embedding a weldable strain gauge	The embedded sensor can detect relevant vibrations
	2022	Binder, Stapff, et al. [32]	16MnCr5	RFID transponder	Wireless sensor-embedded gear	Additively manufactured smart gear with wireless vibration monitoring capabilities	The embedded sensor is fully functional, confirming the feasibility of the method
	2021	Tomaz et al. [33]	Stainless steel (316L)	SAW temperature sensor	Wireless temperature sensing device	Smart structure with passive (wireless) sensing capability	Successfully measured temperatures ranging from 25 °C to 200 °C through a wireless temperature sensor
	2021	Hyer et al. [34, 35]	Stainless steel (316)	Type-K thermocouple	Smart transformational challenge reactor (TCR)	Embedding sensors in Transformational Challenge Reactor (TCR) components	The embedded thermocouples consistently read the temperature data up to 500 °C
	2020	Binder et al. [36]	AlSi10Mg	Resistance Temperature Detector (RTD)	Automated sensor embedding tool	A functional and automated sensor embedding tool	Automatic sensor integration is faster than manual integration. However, manual sensor embedding can improve and stabilize part quality
	2020	Jung et al. [37]	Inconel 718C	Type-T thermocouple	Smart turbine blade	Embedding integrated circuit (IC) components based on plastic circuit boards into a turbine blade	The sensors were shielded from thermal damage and provided accurate data
	2017	Attridge et al. [38]	Inconel 718	Type-K thermocouple	TC-integrated turbine vane	Real-time, in-situ prognosis and diagnosis	A SHM system was established to aggregate temperature sensor data for predicting malfunctions in aerospace applications
EBM	2016	Hossain et al. [39]	Ti–6Al–4 V	Piezoelectric strain sensor	Smart part for SHM	Feasibility of producing smart parts with embedded sensors, eliminating the need for post-processing	Enhanced lifespan of the sensors in harsh conditions allows the smart part to be used in pressure tubes, air/fuel premixing, and turbine blades

Table 1 (continued)

AM method	Year	References	Feedstock material	Sensor	Smart metallic structure (SMS)	Focus	Outcome
Laser DED	2025	Zhong et al. [40]	Inconel 718	Distributed optical fiber sensor	Fiber-sensor-embedded metallic component	Utilization of laser shock peening (LSP) to improve bonding, grain refinement, and high-temperature performance of embedded optical fiber sensors	LSP induced ~ 130 με compressive strain, reduced grain size by 20%, and increased fiber slippage temperature from 252 °C to 305 °C
	2023	Nuñez et al. [20]	Stainless steel (316L)	Type-K thermocouple	Smart part for high-temperature measurement	Investigating the impact of high-temperature laser heating on sensor signal performance	The high-temperature experiments conducted at 350 and 900 °C yielded precise temperature measurements via embedded sensors
	2023	Feldhausen et al. [21]	Stainless steel (316L)	N/A (Only ceramic inserts)	Ceramic embedded AM part without sensor	Fabrication of a multi-component proof-of-concept using hybrid-directed energy deposition	Wet powder may improve mechanical strength and thermal barrier to protect the ceramic insert, and also, the metal layers should be deposited at an oblique angle
	2020	Juhasz et al. [41]	Stainless steel (300-series)	Strain gauge	Smart tensile bar	Fabricate sensor-embedded metallic structures using a hybrid manufacturing process	The embedded sensor measured strain during the tensile tests at room temperature
	2003	X. Li & Prinz [42]	Stainless steel (316L)	FBG strain and temperature sensor	Smart part for temperature and strain monitoring	Temperature and strain measurement	The sensors demonstrated high accuracy, temperature capacity, and sensitivity for both temperature and strain measurements
Wire-arc DED	2025	Huang et al. [43]	Al 5356	RTD and strain gauge	Smart Metal Beam	Development of a "Smart Beam " integrating subsurface strain and temperature sensors for real-time SHM	Embedded RTDs achieved a temperature error of ≤ 0.5%, while SGs reliably recorded strain, confirming accurate sensing performance
	2025	Zhou et al. [44]	Al 5356	Piezoelectric sensor	Self-Aware Structure	Fabricating of a hybrid-manufactured beam with subsurface-embedded PZT sensors for self-aware SHM under mechanical and thermal loading	Embedded sensors exhibited reliable guided-wave responses and stress–temperature sensitivity comparable to those of surface-mounted sensors

Table 1 (continued)

AM method	Year	References	Feedstock material	Sensor	Smart metallic structure (SMS)	Focus	Outcome
UAM	2024	Zhao et al. [19]	Aluminum	FBG strain sensor	Smart strain measuring tool	High-frequency dynamic strain measurements through the embedded FBG sensor	The FBG sensor detected a minimum dynamic strain of 2.5 με and dynamic events up to 10 kHz
	2023	Khattak et al. [22]	Aluminum	Piezoelectric strain sensor	Smart vibration monitoring part	Analyze and assess the effectiveness of the embedded sensor	Theoretical and experimental natural frequencies showed good agreement
	2022	Ramanathan et al. [45]	Aluminum	Piezoelectric strain sensor	Smart non-destructive testing device	Fast production of functionalized metal structures	The Al-PVDF sensor exhibited high linearity and sensitivity
	2022	Hyer et al. [46]	Stainless steel (SS304)	Fiber optic strain sensor and Type-K thermocouple	Smart heat pipe	Embed sensors into the wall of a pipe for temperature and sensor measurement	The measured temperature and strain of the pipe with flowing water exhibited strong agreement with the readings from the external sensors
	2019	Chilelli et al. [47]	Aluminum	FBG strain sensor	Smart crack detection device	Structural health monitoring applications	Embedded FBG sensors can enable early fracture detection and provide monitoring of crack progression
	2019	Petrie et al. [48]	Aluminum	Optical fiber temperature sensor	Sensor-embedded channel	Embed sensors within both straight and curved channels of the component for comprehensive monitoring	Embedded sensors remained fully functional at elevated temperatures (i.e., up to 500 °C)
	2019	Bournias-Varotsis et al. [49]	Aluminum	SMT resistor	3D electronics embedded SMS	Fully embed electronics component in a metal matrix	Encapsulated conductors stayed fully stable at 60 °C, with minimal change up to 100 °C
	2019	Petrie et al. [50]	Aluminum (Al 6061-H18)	N/A (Fiber)	Fiber optical sensor embedded metal part	Embed Cu and Ni-coated fibers into an Al sheet to assess high-temperature survival and bonding integrity	The approach exhibited potential for SHM at harsh environment applications
	2018	Bournias-Varotsis et al. [51]	Aluminum (3003-H18)	SMT resistor	SMT resistor embedded SMS	Embed electronics component into a metal part	The approach enabled the SMS with integrated 3-D electrical circuits
	2015	Monaghan et al. [52]	Aluminum (Al 3003 H18)	N/A (Optical fiber)	Optical fiber-embedded metal part	Embed metal-coated fiber into the part to evaluate fiber bonding and the mechanical strength of the SMS	The embedded fiber remained functional, showing strong bonding with the host metal structure

2.1.1 Temperature sensors

This subsection describes the temperature sensors commonly selected for embedding into metal structures to monitor temperatures. These include Thermocouples (TC), Resistance Temperature Detector (RTD), Fiber Bragg Gratings (FBG), and Surface Acoustic Wave (SAW) sensors.

2.1.1.1 Thermocouples Thermocouples (TCs) are widely adopted in SMS due to their fast response and broad operating temperature ranges. As shown in Fig. 4a, a typical TC consists of a closed loop made of two materials with differing thermal conductivities. When a temperature change occurs, a current flows through the loop, generating a thermoelectric force that allows for temperature measurement [54]. Given their widespread usage, various types of TCs are available from various materials to meet specific temperature ranges and environmental requirements. For instance, Type-K TCs (chromel/alumel) are widely used in industrial applications due to their broad measurement range (−200 °C to 1260 °C) [55]. For moderate temperature measurements, Type-J TCs (constantan/iron) are suitable, covering −40 °C to 750 °C [56]. In low temperature applications, Type-T TCs (constantan/copper) provide a temperature range from −200 °C to 400 °C [57]. For extremely high temperature environments (> 1500 °C), Type-R, S, and B TCs (platinum/rhodium) deliver stable measurements. In addition to specific temperature ranges, certain TC types offer unique advantages. Type-E TCs (chromel/constantan) are valued for their high sensitivity [58], while Type-N TCs (nickel–chromium/silicon) are known for their resistance to oxidation [59], making them ideal for harsh environments.

Table 2 Summary of sensors used in SMS

Sensor	Sensor type	Measurement	Access type	Relevant features	Constraints/Requirements	SMS literature employed the relevant sensor
TC	Type-T TC #	Temperature		Low temperature, fast response, relatively low cost	Electrical insulation	[19, 57]
	Type-K TC #		Wired	Wide measurement range, suitable for industrial application		[55, 56, 59, 89]
	Thin Film TC #			Small size, fast response, suitable for embedding		[90]
RTD	Wire-wound Pt RTD	Temperature	Wired	High temperature, high accuracy, stable measurement	Preventing thermal shock and mechanical impact	[58]
	Thin Film Pt RTD #			Small size, high disturbance resistance, suitable for embedding		[91]
FBG	Standard FBG #	Temperature / Strain	Wired	Electromagnetic interference resistance, high cost	Low temperature embedding process	[50, 60, 61]
	Enhanced FBG #			High temperature, suitable for an extreme environment	Sensitivity to mechanical impact	[54]
	Miniature FBG #			Small size, suitable for embedding		[50, 53]
	RFID-based FBG		Wireless	Wireless monitoring		[92, 93]
SAW	High-Temperature SAW Sensors #	Temperature / Strain	Wired	High temperature, suitable for extreme environment	Smooth attachment surface required	[33, 59]
	Miniaturized SAW #			Small size, suitable for embedding and integration		[33]
	RFID-based SAW #		Wireless	Wireless monitoring, suitable for integration		[39]
SG	Foil SG #	Strain	Wired	Low cost, high applicability, suitable for most industries, and research	Low-temperature tolerance of sensor packaging materials Electrical insulation requirement	[63, 94]
	Thin Film SG #		Wired	Small size and thin thickness, suitable for precision MEMS		[95]
	RFID-based SG		Wireless	Wireless monitoring, suitable for embedding		[92, 93]
Piezoelectric sensor	PZT (Lead zirconate titanate)#	Strain	Wired / Wireless	High sensitivity, high frequency strain and vibration detection	Brittle, piezoelectric coupling, and Curie temperature limitation	[96]
	PVDF (Polyvinylidene Fluoride) sensor #		Wired / Wireless	Flexible, suitable for a low-stress environment		[97]
	Quartz sensor		Wired / Wireless	High stability, suitable for the detection of precision vibration and strain		[98]
Motion sensor	Accelerometers #	Vibration	Wired / Wireless	Detection for impact and vibration, especially for SHM	Demands enhanced electronics shielding and careful wiring integration	[99]
	Ultrasonic sensor	Distance	Wireless	Distance measurement and position sensing, suitable for robotics and automation system		[100]

[# indicates the sensors used in the AM of SMS]

Among various types of TCs, Type-K has found a widespread application in the AM of SMS [20]. Despite their advantages, TCs can encounter accuracy and stability issues at low temperatures (i.e., < 200 °C), which limits their effectiveness in SMS applications operating under low-temperature conditions [35].

2.1.1.2 Resistance temperature detectors (RTDs) As an alternative to TCs, RTDs have gained significant attention owing to their ability to provide more accurate temperature readings over a wide range of operating temperatures. Most RTDs are made of fine, coiled wires encased in ceramic or glass (see Fig. 4b). The wire materials are typically platinum (Pt), nickel (Ni), or copper (Cu), as these metals exhibit a precise, accurate relationship between temperature and resistance [60]. The working mechanism of RTDs is the same as resistors; the variance of measuring temperature has an accurate, stable, and predictable model with the material used as resistors. The most commonly used RTDs

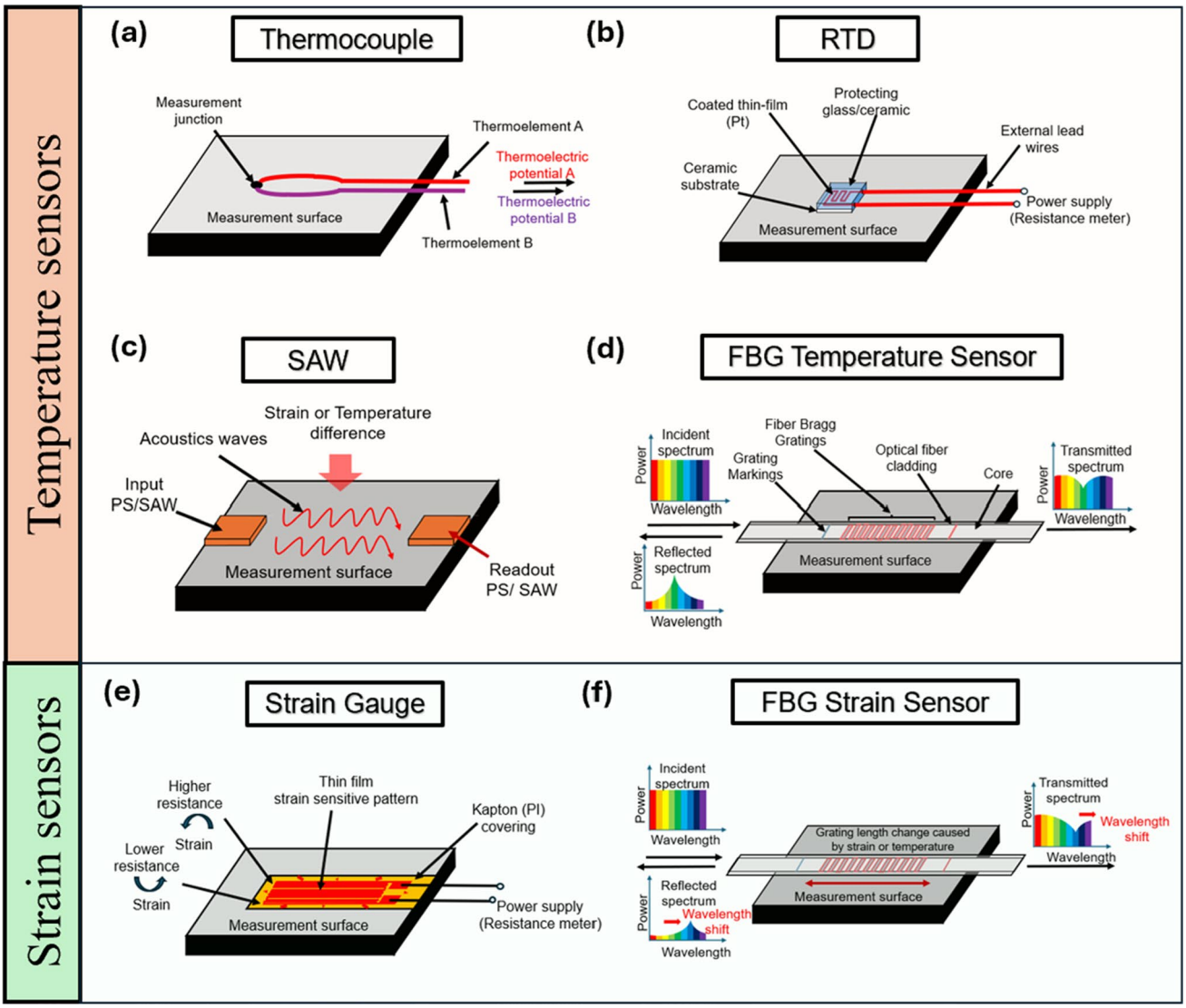

Fig. 4 Schematic of the temperature and strain sensors widely used in SMS; **a** Thermocouple (TC); **b** Resistance temperature detector (RTD); **c** Surface acoustic wave (SAW): **d** Fiber bragg grating (FBG) temperature sensor; **e** Strain gauge (SG); and **f** FBG strain sensor

contain thin and fine coiled wire, which is wrapped around an electrical material with poor conductivity like ceramic or glass and is shielded by materials with higher melting temperatures (usually glass) to protect the fine wire from external disturbances or destruction. The Pt-RTD is the most widely used RTD sensor due to its high repeatability, accuracy, and broad operating temperature range (−200 °C–860 °C) [65]. While most RTDs outperform TCs, Ni- and Cu-based RTDs have lower oxidation resistance than Pt-based RTDs. As such, careful sensor selection is essential for specific applications.

2.1.1.3 Surface acoustic wave (SAW) sensors SAW sensors measure temperature by detecting changes in the propagation characteristics of surface acoustic waves, caused by the material's elasticity and dimensions (Fig. 4c). The key acoustic wave characteristics detected by SAW sensors are transfer velocity and frequency. Two common types of SAW sensors for temperature measurement are resonator-based and delay-line SAW sensors. Resonator-based SAW sensors reflect temperature variations in shifts of the resonant frequency. The detectable temperature range depends on the piezoelectric materials used, such as $LiTaO_3$ and $LiNbO_3$, enabling maximum temperatures between 500 °C and 1000 °C [61]. Delay-line SAW sensors, on the other hand, measure the time delay of surface waves traveling between two transducers. Variations in wave velocity can arise from dif-

ferences in materials (e.g., Pt-based alloys or Ir–Rh alloys) and electrode thicknesses [62].

2.1.1.4 Fiber Bragg grating (FBG) sensors Unlike TCs and RTDs, which rely on electric properties and are vulnerable to electromagnetic interference (EMI), FBG sensors measure temperature by detecting shifts in the Bragg wavelength. As temperature changes, the wavelength of light reflected within the optical fiber shifts, enabling precise temperature estimation [63] (see Fig. 4d). FBG sensors offer several advantages over TC and RTD due to their light-based working mechanism. They provide highly accurate and precise temperature readings, distributed sensing capabilities (e.g., multiple sensors along a single optical fiber), and maintain fidelity in harsh EMI environments [64]. However, these benefits come with challenges, including the high cost of FBG sensors and the complexity of embedding them into metallic components [65].

2.1.2 Strain sensors

Strain sensors commonly used in SMS include Strain Gauges (SG), FBGs, Piezoelectric sensors (PS), and SAW sensors. Each of these sensor types is described in detail in the following subsections.

2.1.2.1 Strain gauges Strain gauges (SGs) are a widely used strain sensor in SMS owing to their high sensitivity, compact size, and ease of integration into various metallic structures [66]. It operates based on the principle of electrical resistance change under mechanical deformation, allowing for precise measurement of strain in response to applied stress (Fig. 4e). The core component of an SG is a serpentine resistive wire pattern, typically made from materials such as constantan (Cu-Ni), Cr-Ni, or Fe–Cr-Al [67]. The packaging materials commonly used include polyimide (PI), polyester (PE), or glass-reinforced epoxy-phenolic [68]. Among these, Cu-Ni SGs with PI carrier are widely used in commercial applications and are suitable for static strain measurements at temperatures up to 300 °C [69]. In contrast, unpackaged Fe–Cr-Al SGs are ideal for dynamic strain measurements at temperatures as high as 1150 °C, although they require additional electrical insulation [70].

To meet the demands of SMS, thin-film SGs are preferred due to their ability to be directly deposited onto AM structures with a minimal footprint, thereby reducing parasitic effects under structural loading. With a thickness of approximately 20 µm—significantly thinner than the 200 µm of conventional foil or wire strain gauges [71]— thin-film SGs greatly enhance bonding performance in MAM, making them a critical element in SMS [66].

2.1.2.2 FBG strain sensors In addition to temperature measurement, FBG sensors are capable of measuring strain. Mechanical stress and strain cause changes in the grating period of the fiber (Fig. 4f), which are detected to measure strain [72]. The FBG sensors can operate within a wide temperature range of −200 °C to 1000 °C [73], making them suitable for SMS. The multifunctionality of FBG sensors offers significant advantages in enhancing the mechanical properties of SMS components by reducing the number of embedded sensors. By integrating multiple FBGs for strain and temperature measurement within a single optical fiber, the intrusion of the sensor network is minimized, further optimizing the structural integrity of the system.

2.1.2.3 Piezoelectric sensors (PS) and SAW sensors PSs and SAWs sensors measure strain by analyzing wave signals affected by stress or load variations [74, 75]. These sensors operate based on the piezoelectric effect, where mechanical energy, such as strain or pressure, is converted into electrical signals. This unique property makes them particularly suitable for both static and dynamic strain measurements, offering versatility across a range of applications [76]. The capability of PS and SAW sensors to detect subtle changes in mechanical strain with high sensitivity and reliability has made them valuable tools SHM [77]. In addition, their compact size, fast response time, and non-intrusive nature contribute to their adaptability in real-world environments, including aerospace, automotive, and advanced manufacturing systems. Another significant advantage of these sensors is their ability to operate across a wide temperature range. Additionally, specialized PSs (e.g., $(1-x)$ $BiScO_3-xPbTiO_3$ (BSPT)) are capable of strain-sensing at temperatures between 400 °C [78] and 600 °C [61]. This thermal resilience allows PS and SAW sensors to perform reliably in harsh conditions, such as high-temperature industrial processes and environments encountered in energy or aerospace applications.

2.1.3 Other sensors

In addition to strain and temperature sensors, various motion sensors can be integrated into SMS. Sensors such as accelerometers [79], ultrasonic sensors [80], passive infrared sensors [81], microwave sensors [82], and tomographic sensors [82] can detect subtle movements, anomalies, deformations, and vibrations in SMS. These motion sensors can expand the functional capabilities of SMS by enabling comprehensive

monitoring and real-time feedback, which are critical for maintaining structural integrity and performance.

Besides, recent studies have demonstrated that inherently functional materials can impart self-sensing capabilities to metallic structures, as those materials themselves retain natural strength for sensing. For instance, piezoresistive, pyroelectric, and thermoresistive materials have been used to build SMS that can monitor their strain, temperature, or stress state through intrinsic electrical or thermal responses [83, 84]. These studies highlight the promise of integrating sensing functions directly into structural materials, which minimizes wiring complexity and enhances durability. However, challenges remain in achieving stable signal calibration under cyclic loading and extreme temperature environments.

Moreover, to further enhance self-sensing capabilities and optimize the embedding process, active metal-matrix composites incorporating shape memory alloys have been developed to enable both actuation and sensing functions within the same structure [85]. Such strategies offer tunable stiffness and adaptive responses to external stimuli. However, their implementation in large-scale metallic components remains limited due to cost and integration constraints.

Another promising direction involves the integration of eddy current sensors for non-contact defect detection and displacement monitoring [86]. Eddy current–based approaches might be particularly advantageous for metallic systems, offering robustness under harsh conditions. Nevertheless, their sensitivity could be degraded when the sensors are embedded deep within conductive layers. Overall, these advances suggest that the next generation of SMS will likely combine both material-embedded self-sensing mechanisms and hybrid sensor networks to achieve higher levels of functionality and reliability. Future research should focus on unifying signal calibration frameworks and developing robust data-driven fusion models to interpret complex multi-sensor responses in realistic structural, environmental, and operating conditions.

2.1.4 Key considerations for sensor embedding into metal structures

The diversity of SMS fabrication processes introduces specific constraints and requirements for embedding different types of sensors, depending on both the involved materials, interfaces, and sensing principles. These factors directly affect the compatibility of sensors with a given fabrication pathway and, consequently, the overall design of SMS. Hence, selecting suitable manufacturing and embedding methods requires a comprehensive evaluation of both sensor materials and their operating mechanisms.

For temperature sensors, both TCs and RTDs rely on metallic conductors and can withstand relatively high temperatures. This can make them compatible with various metal AM processes, provided that the sensor body is not directly exposed to the molten pool for extended periods. In contrast, the behavior of optical and acoustic sensors (e.g., FBS, SAW) is markedly different. FBGs composed of silica fibers and operating based on Bragg wavelength shifts are highly sensitive to temperature and residual strain [19]. Consequently, they are not suitable for direct exposure to fusion-based processes such as DED or LPBF.

Similarly, the processing compatibility of SGs depends strongly on their design. Conventional foil SGs consist of metallic resistive grids mounted on polymer carriers (e.g., polyimide), which limit their maximum embedding and operating temperatures. As such, they are better suited for adhesive bonding or low-temperature thin-film deposition on prefabricated metallic components, followed by the application of a thermal shielding layer prior to resuming the AM process. Although high-temperature SGs have been developed [87], they require robust electrical insulation and precise control of coating thickness to prevent delamination during thermal cycling. PZT-based sensors combine high piezoelectric coupling with inherent brittleness [77], necessitating the use of a compliant interlayer for mechanical protection when embedded in metallic structures. Moreover, their limited Curie temperature must be carefully considered, as prolonged exposure to elevated temperatures can lead to polarization loss and degradation of piezoelectric performance [88]. Other sensor modalities (e.g., accelerometers, microwave sensors, tomographic sensor arrays) typically contain delicate electronic components. In all cases, the embedding strategy must provide sufficient thermal and mechanical protection while maintaining reliable signal transmission paths.

Table 2 summarizes the main sensor types discussed in Section 2.1, along with their sensing mechanisms, access modes, key features, and associated SMS processing constraints or requirements. This comparison highlights that no single fabrication method can accommodate all sensor types; instead, the processing window of SMS must be tailored for each sensor to preserve functionality while achieving desired structural performance.

2.2 Metal additive manufacturing methods for SMS

As shown in Fig. 5, MAM technologies can be classified into two main categories: (i) phase change (melted) and (ii) solid-state (unmelted). These categories can be further subdivided based on the type of thermal energy source employed. While a wide range of AM methods exist, as listed in Fig. 5, the available literature indicates that only six MAM

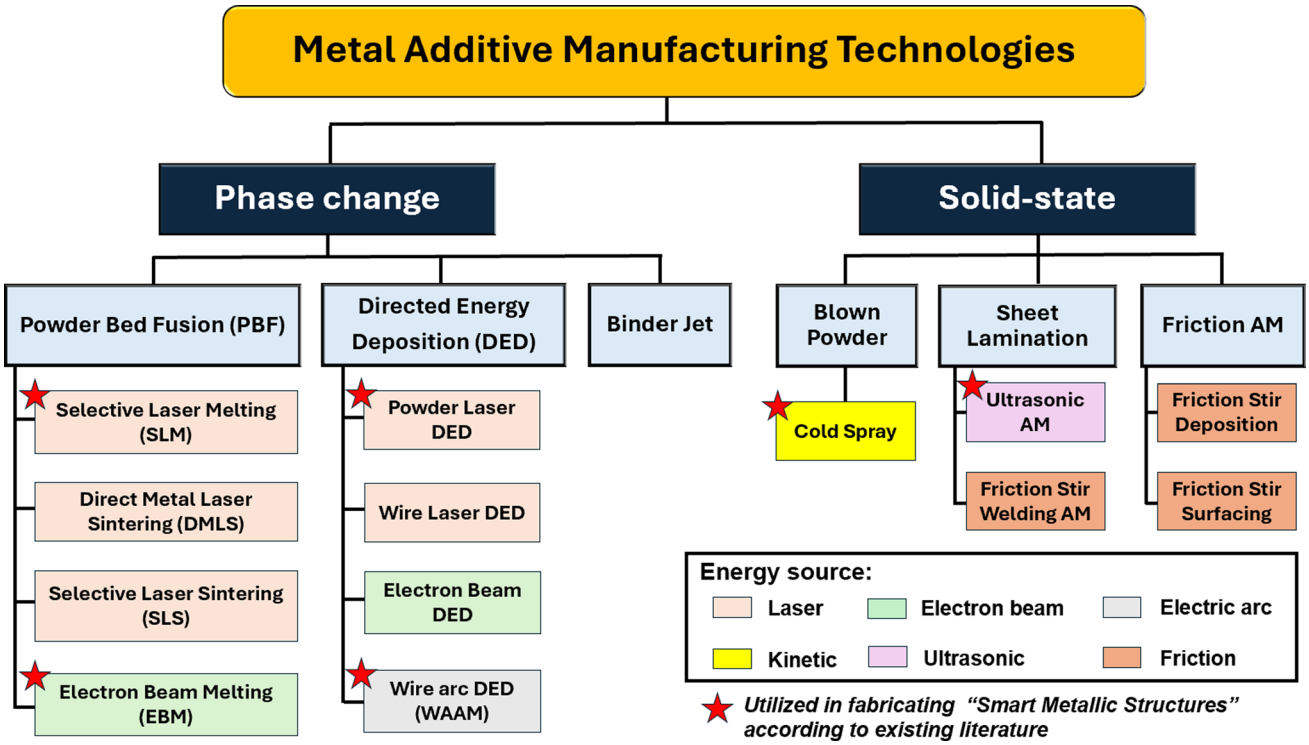

Fig. 5 Classification of metal AM technologies

techniques have been applied in the domain of SMS, which include: (1) laser powder bed fusion (LPBF); (2) electron beam melting (EBM); (3) laser-directed energy deposition (DED); (4) wire-arc DED also known as wire-arc additive manufacturing (WAAM), (5) ultrasonic additive manufacturing (UAM); and (6) cold spray additive manufacturing (CSAM). Among these methods, CSAM has primarily been utilized for surface metallization or coating applications rather than for constructing the bulk host structure [43, 44]. Therefore, in this context, CSAM was excluded from the comparative analysis of structural embedding approaches, though it remains a promising technique for functional surface integration and hybrid manufacturing strategies. The relative distribution of these techniques within the SMS domain is shown in Figs. 6a–b, in which laser-DED and wire-arc DED are collectively categorized under the DED classification. Additionally, Table 3 summarizes the key characteristics of these major AM processes, including their technical features, compatible feedstock materials, and their respective advantages and limitations for AM applications. Meanwhile, several other MAM approaches remain unexplored in this context, as shown in Fig. 6c.

To date, most research on sensor-embedded SMS has focused predominantly on LPBF [16–18, 30–38], with only a limited studies employing EBM [39]. This concentration suggests that LPBF is currently regarded as the most viable approach for producing SMS, likely due to its high precision, material compatibility, and ability to achieve complex geometries. Following LPBF, UAM is the second most widely used technique for SMS production. UAM offers several advantages, including low processing temperatures and rapid fabrication cycles, making it well-suited for embedding sensors into delicate components and for bonding dissimilar metals [52]. However, UAM has limitations when applied to host metals with thick cross-sections or high-melting temperatures. DED has also been utilized to embed sensors into metal structures, primarily due to its high deposition rates and compatibility with a wide range of alloys [101, 102]. Nevertheless, current research in DED has primarily focused on powder-based DED and wire arc DED (i.e., WAAM), while wire laser DED and electron beam DED remain largely limited for SMS.

The following section (Section 3) provides a detailed overview of additively manufactured SMS produced using each of these techniques, covering their fabrication processes, sensor integration strategies, material compatibility, and performance outcomes.

3 Sensor embedding and fabrication of SMS

This section discusses the sensor embedding and fabrication of SMS using the MAM techniques. It comprehensively summarizes the processes involved for each MAM method,

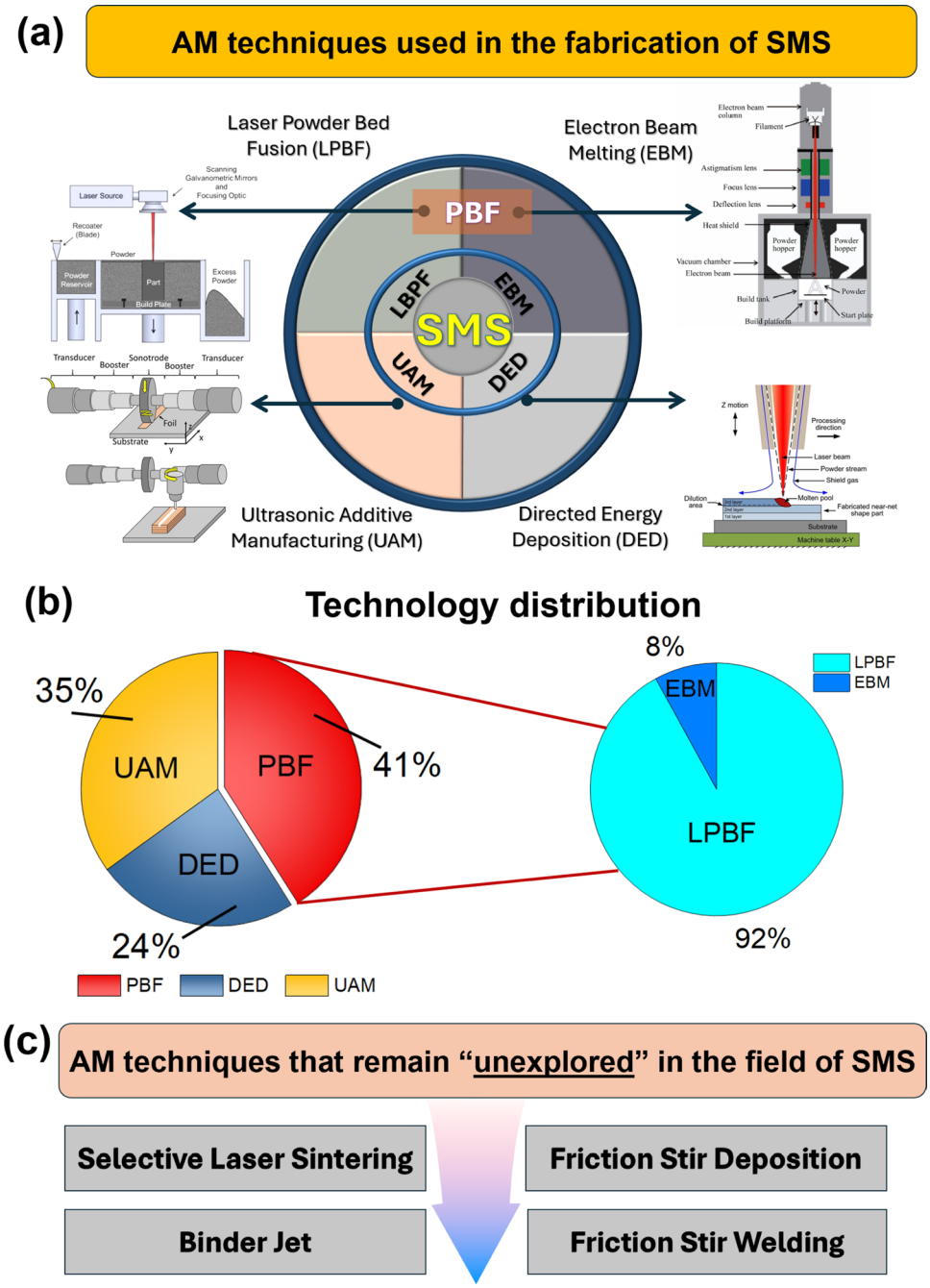

Fig. 6 **a** Metal additive manufacturing (MAM) techniques applied to SMS to date; **b** Distribution of different AM technologies within the field of SMS; **c** AM technique that remains unexplored in the SMS domain

including sensor embedding, sensor packaging (e.g., heat-shield application), metal layer restoration, AM resumption, post-machining processes, and sensor data verification.

3.1 SMS fabricated via powder bed fusion (PBF)

PBF is among the most widely utilized methods for fabricating SMS, with LPBF being the predominant method in this domain (see Fig. 6b, right panel). Various SMS have been successfully produced using PBF, including: a wireless sensor-embedded gear, a wireless temperature sensing device, a smart injection molding tool, a smart turbine blade, a smart transformational challenge reactor, a smart vibration detector, a smart part for structural monitoring, etc. (see Fig. 7).

Notably, several studies focused on the fabrication of SMS with embedded wireless sensors [17, 32, 33, 36–38]. Tomaz et al. [33] developed a wireless sensor-based SMS using LPBF with stainless steel (316L). This study focused on the design, fabrication, and validation of a real-time temperature sensing device, which is capable of sensing and storing real-time temperature data. The Surface Acoustic Wave (SAW) temperature sensor (*Model: SS2467BB2*) used

Table 3 Overview of AM methods used in the fabrication of SMS [*# symbol denotes feedstock material that has been used to date in AM of SMS*]

AM method	Technical properties	Feedstock material	Advantages	Limitations
Laser powder bed fusion (LPBF) 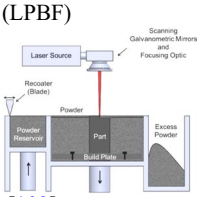 [103]	Heat source: laser Laser power range: 50–1000 W [104–106] Beam size: 35–140 μ m [104, 107] Laser scanning velocity: 0.1–2.5 m/s [106, 108, 109] Feedstock: powder Powder size: 20 – 100 μ m [110, 111]	*#Al alloys* *#Ti alloys* *#Fe-based alloys* *#Ni-based super alloys* *#Tool steels* Mg alloys MMCs High-entropy alloys	High-quality surface finish [112] Production of intricate geometries [113] High-density and well-bonded structures [114] Low material wastage and powder reusability [114]	Limited material options [115] Residual stresses and warping [116] Complex microstructure [117] Relatively slow and long processing time [118] Inert gas requirement [119]
Electron Beam Melting (EBM) 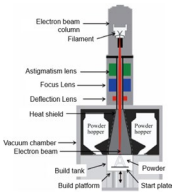 [120]	Heat source: electron beam Power range: 30–42 kW [121] Beam size: 50–150 μ m [122] Feedstock: powder Scanning velocity: 3.3–5 m/s [122, 123]	*#Ti alloys* Al alloys Mg alloys Fe-based alloys Co-based alloys High-entropy alloys Cu and Cu-alloys W–Ni-Fe alloys MMCs	High production rate [124] High-temperature capability [125] Reduced residual stress [121] Strong mechanical properties [125] Less porous AM parts [126]	Limited material selection [127] Low fatigue life [127] Vacuum requirement [127] High energy consumption [128] High equipment and maintenance costs [129]
Laser-directed energy deposition (LDED) [130] 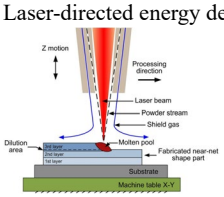	Heat source: laser Power range: 300–6000 W [104, 131] Beam size: 0.5–6 mm [104] Scanning velocity: 0.6–500 mm/s [131, 132] Feedstock: powder Powder feed rate: 5–10 g/min [104, 133]	*#Fe-based alloys* Ti alloys Mg alloys Ni-based alloys Co-based alloys High-entropy alloys Cu and Cu-alloys MMCs	Multi-material capability [134] Printing functionally graded materials [114] Large build size with high-deposition rate [135] Part repair and remanufacturing [136] Customizable deposition paths [136] Less post-processing for machining [137]	Surface finish and precision [138] Heat-affected zone [139] Residual stresses [140] Requirement for inert gas [102] Material efficiency [141] Equipment and operational costs [137]
Wire-arc DED (i.e., WAAM) 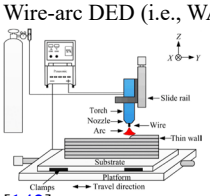 [142]	Heat source: Electric arc [143] Power range: 2 – 30 kW [143] Deposition rate: 2 – 8 kg h^{-1} (> 10 000 mm^3 min^{-1}) [144] Layer thickness: ≈ 1 mm typical [144] Wire feed rate: 1 – 10 m min^{-1} with shielding gas (e.g., Ar, He) [145] Process control: Robot/CNC motion [145]	*#Al-based alloy* [144] Fe-based alloys [144] Ni-based super alloys [145] Ti-based alloys [144] Cu-based alloy [145]	High deposition rate (up to 8 kg h^{-1}) [144] Large build volume (> 1 m^3) and low equipment cost [143] Deposition efficiency > 95% [145] Suitable for repair and remanufacturing [145] Good mechanical properties with controlled heat input [144]	Poor surface finish (Ra > 0.8 mm) requiring post-machining [143] Residual stresses and distortion from high heat input [145] Porosity and micro-cracks [144] Limited dimensional accuracy (± 1 mm) [143] Anisotropic microstructure and coarse grains due to directional solidification [144]
Ultrasonic additive manufacturing (UAM) 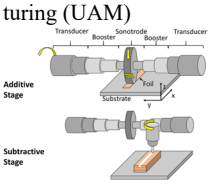 [146]	Heat source: ultrasonic wave Power range: 1–9 kW [147] Scanning velocity: 400–1000 mm/s [148] Feedstock: metal foil/sheet	*#Al alloys* *#Fe-based alloys* Ti alloys Cu and Cu alloys Mg alloys Ni alloys	Low-temperature process [149] Reduced thermal effects [150] Minimal residual stresses [151] Dissimilar material joining [152] High-dimensional accuracy [152] Eco-friendly process [149]	Limited material selection—*not compatible with the hard steels and nickel* [153] Thickness limitations [154] Inconsistent bonding [155] Limited build volume and speed [156] Low production scale [157]

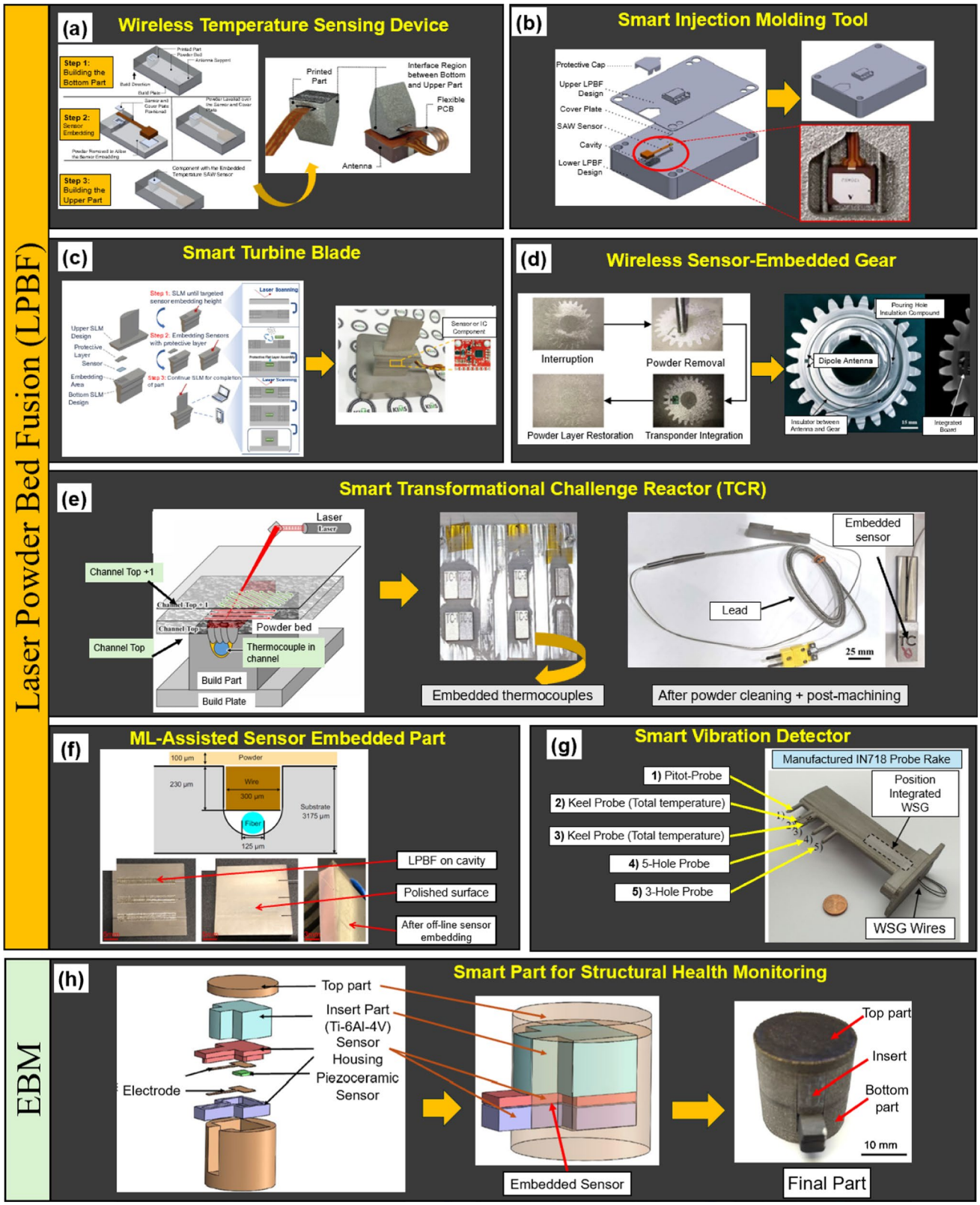

Fig. 7 SMS fabricated using PBF techniques: **a** Wireless temperature sensing device [33]; **b** Smart injection molding tool [17]; **c** Smart turbine blade [37]; **d** Wireless Sensor-embedded gear [32] **e** Smart transformational challenge reactor (TCR) [35]; **f** ML-Assisted Sensor Embedded Part [16]; **g** Smart Vibration Detector [31]; and **h** Smart part for SHM [39]

in this study operated within a temperature range of −40 to 200 °C. As depicted in Fig. 7a, the authors employed a method that involves an interruption of the LPBF process to add the sensor and corresponding cover plate. The printing process was then resumed until the entire part was printed. Although there were gaps between the cover plate and the main body, which could potentially affect the mechanical properties of the component, the embedded SAW sensor successfully measured temperatures ranging from 25 °C to 200 °C via its wireless system. The temperature recorded by the embedded SAW sensor was validated by an external Resistance Temperature Detector (RTD), confirming the full functionality of the SMS.

Šakalys et al. [17] used LPBF with stainless steel (316L) to embed a wireless SAW temperature sensor (*Model: SNT2427BB2*) into an injection molding tool for temperature monitoring (Fig. 7b). The sensor can measure temperatures from −40 to 200 °C, making it suitable for various injection molding applications. The sensor embedding process involved multiple steps. First, the LPBF process was paused to vacuum clean and expose the sensor cavity, where the sensor was placed and covered with a heat shield. After resuming LPBF, a protective cap and silicone sealant were added to make the sensor watertight and shield it during machining. The tool had 99.9% density, no defects, and the sensor functioned well for real-time temperature monitoring. Despite some minor design challenges, the sensor retained full functionality after post-processing and was able to accurately record temperature data throughout the injection molding process, demonstrating its potential for real-time process control and monitoring. For future research, the authors recommended positioning the sensor in the opposite direction from the cooling pipelines to prevent signal disruptions. They also suggested using a smaller sensor antenna to enhance the sensor's flexibility.

Jung et al. [37] utilized LPBF with Inconel 718C to fabricate a smart turbine blade for wireless acceleration and temperature monitoring of the turbine blade via Bluetooth (Fig. 7c). The sensor system included a transistor-type TC sensor (*Model: LM35DZ*) and an Integrated Circuit (IC) chip (*Model: MPU6050*). They first embedded a TC sensor in a stainless-steel part to validate temperature data, then embedded a PCB-based acceleration IC into the turbine blade. The process involved pausing printing, cleaning the sensor cavity, inserting the sensor with protection, and resuming printing. The final blade's mechanical properties were unaffected, and real-time data were successfully recorded and validated, demonstrating its potential for intelligent status analysis.

Binder et al. [32] integrated a wireless sensor system into a gear produced via LPBF using alloyed steel (16MnCr5) (Fig. 7d). The study focused on designing and validating an RFID antenna for gear performance monitoring. The system included a comprised an ultra-high frequency (*UHF, 868 MHz*) RFID unit, a mid-range reader (*Pulsar MX*), and an accelerometer (*Kionix, KX122*). During the process, printing was paused, excess powder was removed, and the sensor was placed into the cavity. The antenna was manually soldered to the sensor for better communication, and the cavity was refilled. The "sensor-monitored gear" (i.e., smart gear) successfully transmitted acceleration data, though the readout range was limited to 1 cm due to electromagnetic interference, highlighting challenges in RFID use in metal environments. Despite this limitation, the implementation of the sensor-monitored gear aimed to address several key technical challenges in the field, including: (i) RFID applications in electromagnetically shielded metal environments; (ii) AM of antenna and loaded component in one process; (iii) AM of the conductive path between antenna and the sensor; and (iv) integration of the RFID transponder during the LPBF manufacturing process.

Several other studies have also utilized LPBF for the fabrication of SMS with passive sensing capabilities. Binder et al. [36] employed LPBF with AlSi10Mg to automate sensor embedding in an AM component. They developed an approach where a suction cup removed excess powder from a sensor cavity during the process interruption, and a kinematic system inserted an RFID tag using a vacuum gripper. Attridge et al. [38] used LPBF with Inconel 718 to fabricate a TC-integrated turbine vane for temperature sensing with a tolerance of ± 2 °C. After producing the vane, they applied a stainless-steel coating via cold spray, cleaned excess powder from the grooves, welded Type-K TCs into the grooves, and sealed them with IN718 powder. Both approaches successfully integrated sensors for effective temperature monitoring.

In addition to SMS with wireless embedded sensors, there are studies in the literature [16, 31, 34, 35] that have employed LPBF to fabricate SMS featuring active sensing. Hyer et al. [34, 35] developed TC embedded structures by LPBF with stainless steel (*316*). The objective of the study was to create a smart metallic structure compatible with the components of the transformational challenge reactor (TCR) (Fig. 7e). A Type-K TC was used as the embedded sensor, featuring a stainless steel (316) sheath, and its internal leads were insulated with magnesium oxide. The LPBF process was not interrupted for sensor insertion (i.e., off-line sensor insertion). Channels were first drilled into the build plate, and sensors were spot-welded into place, staying clear of the powder raking process. The structure was built over the sensors, with laser dwell times optimized to reduce porosity. The structure can measure temperatures up to 500 °C, and the embedded TC performed similarly to reference ones

during thermal testing, with minimal differences in reaction time.

Recently, Wang et al. [16] fabricated a Fibre Bragg Grating (FBG)- sensor-embedded smart metallic part using LPBF of a titanium alloy (Ti-6Al-4 V) (Fig. 7f). The FBG sensor, developed with a machine learning-assisted approach, achieved high spatial resolution (28.8 µm) for thermal distribution. The embedding process involved engraving a cavity with wire EDM, placing a fiber inside, filling it with Ti-6Al-4 V wire, and depositing a 100 µm-thick layer before polishing. The C-FBG sensor was then inserted offline and successfully collected real-time thermal data during the LPBF process, recording the temperature profile at different times and locations at the sub-surface level.

Besides temperature sensors, several studies have explored the integration of SGs into metal AM parts for vibration sensing and SHM. Binder et al. [31] used LPBF with Inconel 718 alloy to build a smart vibration detector with an embedded SG (Fig. 7g) for a flow measurement system, where the surrounding flow generates vibrations that are difficult to measure. A weldable SG (*Model: LS31HT*) was used, with its measuring grid placed on a metal plate. After producing the test specimen and cleaning excess powder, the SG was welded to the cavity surface and embedded. The system successfully detected vibrations according to the MIL STD 810 H standard [158], and the data was validated by an external FBG-SG, confirming the effectiveness of the embedded system.

Most recently, Rodrigues et al. [30] fabricated a NiTi–AlSi10Mg smart structure through LPBF. The fabrication sequence involved: (i) fabrication of AlSi10Mg specimens using LPBF with a 0.5 mm hole for sensor embedding under argon protection; (ii) insertion of a 0.5 mm superelastic NiTi wire into the printed cavity after fabrication; and (iii) post-heat treatment at 300 °C for 2 h (Ar/N_2 atmosphere) to enhance interfacial bonding and relieve residual stresses while avoiding brittle Al_3Ni/Al_3Ti phases. The embedded sensor maintained its phase transformation and showed a resistivity change from 8.37×10^{-7} to 9.50×10^{-7} Ω·m (0–2.5% strain), which demonstrates a stable in-situ strain-sensing performance.

In addition to LPBF, EBM was also utilized to produce SMS. Hossain et al. [39] fabricated a smart structure with an embedded strain sensor using EBM and a titanium alloy (Ti–6Al–4 V). The sensor material was piezoelectric ceramic (lead zirconate titanate), which was capable of sensing strain, force, and pressure. The EBM process was paused after completing the bottom part to insert the sensor and its alumina housing, which provided thermal shielding and secure placement (see Fig. 7h). The assembly was aligned in a mask plate before resuming the EBM process. Despite some limitations, such as attachment and bonding strength, the embedded sensor maintained full functionality and durability, proving its potential for aerospace, automotive, and biomedical applications. Notably, the embedded sensors exhibited enhanced lifespan under harsh conditions such as a corrosive environment, high pressure, and high temperature.

Fig. 8 SMS fabricated using DED technique: **a** Smart part for high-temperature measurement [20]; **b** Smart part for temperature and strain monitoring [42]; **c** Smart tensile bar [41]; and **d** Ceramic embedded AM part without sensor [21]; **e** Smart metal beam [43]; and **f** Self-aware structure [44]

3.2 SMS fabricated via directed energy deposition (DED)

DED has emerged as one of the most promising AM route owing to its versatility in processing a wide range of metals and alloys, high deposition rates, and ability to produce large, functional components. Within this family, laser-based DED and wire-arc-DED (i.e., also known as wire-arc additive manufacturing (WAAM)) represent two primary processes that have been reported for SMS fabrication. This section reviews recent developments in SMS fabricated using these two DED-based approaches, with a focus on their underlying processing characteristics, material–sensor compatibility, and strategies for achieving reliable sensor integration within metallic systems.

3.2.1 Laser directed energy deposition (L-DED)

Nuñez et al. [20] fabricated a smart part for temperature measurement by using powder DED with stainless steel (316L). The sensor system comprised commercial Type-K TC. The sensor embedding process, illustrated in Fig. 8a, involved pausing the DED process after fabricating the base and standoff. A groove was then machined into the base to accommodate the sensor. The DED process was subsequently resumed and continued until the top component was completed. Two different configurations were developed using this method: one with an embedded sensor tip and the other with an exposed sensor tip. Both configurations withstood high-temperature performance tests. However, a deflection of the sensor tip was observed due to the high process temperature. Despite this structural deflection, the embedded TCs demonstrated good accuracy during tests at 350 °C and 900 °C, with a deviation of less than 0.75% from the target temperature. Additionally, optimization results indicated that the process could be further refined to minimize sensor tip deflection, improve contact between the host material and the sensor, and reduce porosity by adjusting the contour scan speed and part geometry.

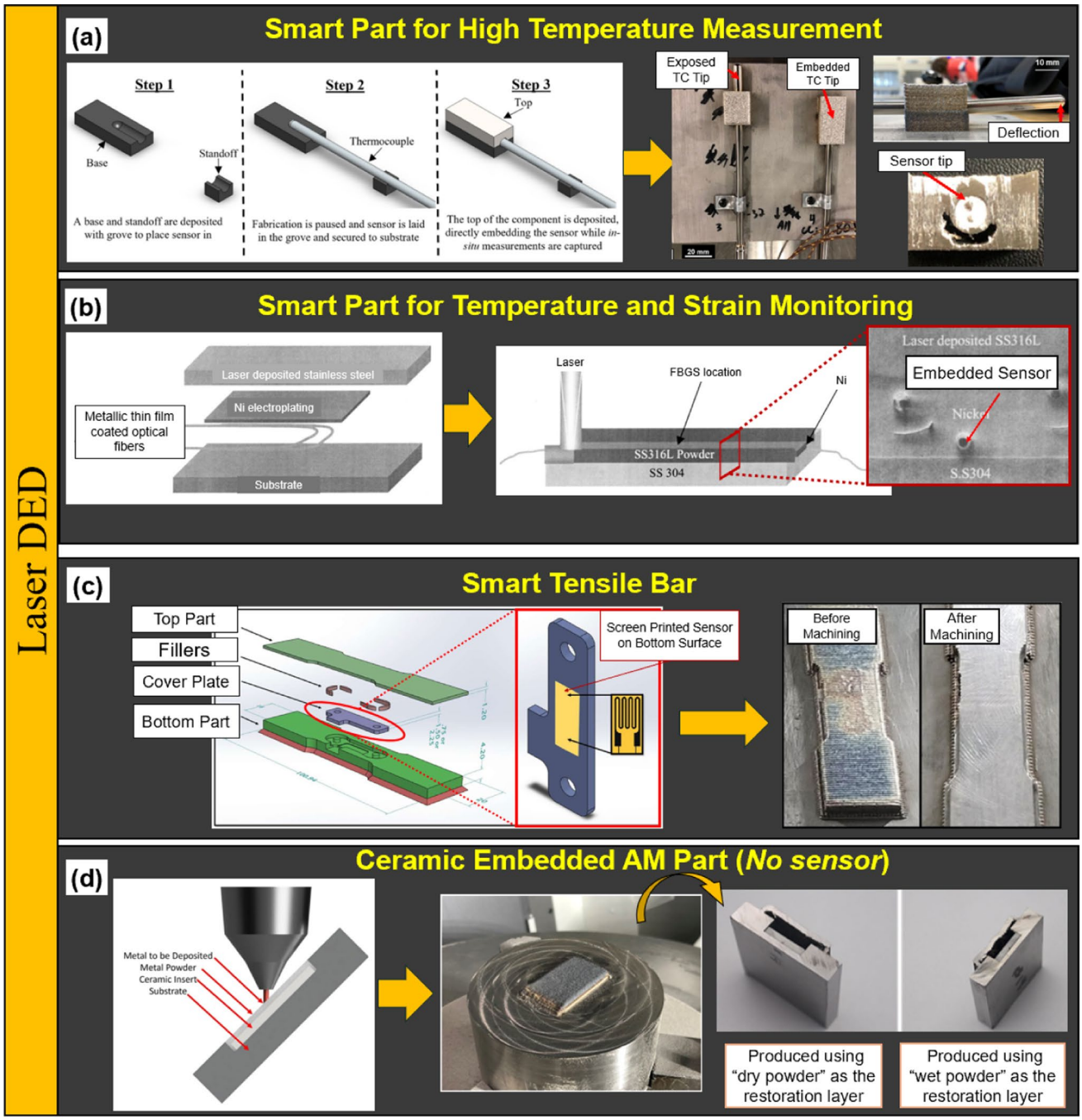

In addition to temperature sensors, two studies have explored the embedding of strain sensors into metal AM parts. Li et al. [42] developed a smart part for temperature and strain measurement using powder-DED of stainless steel (316L) (see Fig. 8b). The sensors, coated with a nickel thin film for thermal shielding, were placed on a stainless steel (304) substrate, followed by electroplating with nickel and DED to complete fabrication. The embedded sensors showed high accuracy and sensitivity. The FBG temperature sensor had higher temperature capacity and sensitivity, while the strain sensor demonstrated good agreement with external FBG sensors. Furthermore, this study employed a decoupling approach to effectively separate the effects of strain and temperature for the embedded FBG sensors.

Juhasz et al. [41] developed a smart tensile bar (Fig. 8c) with DED of 300-series stainless steel. The sensor used was screen-printed ink-based piezoresistive SG. The sensor embedding process involved fabricating the bottom part of the tensile bar, machining it for sensor placement, and adding a 40 µm-thick Zirconia insulation layer. The SG was inserted, stitch-welded, and the DED process was resumed to fill voids and complete the tensile bar. The embedded strain gauge performed accurately during tensile testing, showing potential for SHM and adaptability for embedding sensors in complex structures.

Feldhausen et al. [21] embedded ceramic material within a stainless steel (316L) structure to evaluate the feasibility of resuming DED on the ceramic layer. Unlike other studies, no sensor was used in this study; only ceramic material was embedded within the metallic structure. The ceramic embedding process, outlined in Fig. 8d, involved the following steps: (1) A cavity was machined into the substrate, and the ceramic insert was placed inside the cavity; (2) unmelted metallic powders were used to fill the cavity for process resumption. In one approach, dry powder was used, while in another, the metal powder was wetted with machining coolant to improve adhesion and stability. (3) DED was resumed over the metal powder to complete the structure. To protect the ceramic insert from the high temperatures of the DED process, the authors tilted the substrate at a 35° oblique angle. The integrity of the embedded ceramic was verified using the X-ray computed tomography system. The authors proposed that this method could be adapted to embed various sensors, such as SGs, TCs, and fluidic valves, within metal components for SHM.

Zhong et al. [40] fabricated fiber sensor–embedded Inconel components by combining electroplating, LDED method, and laser shock peening (LSP). The fabrication process included: (i) cleaning and sputter-coating copper-coated silica fibers (125 µm core, 20 µm Cu layer); (ii) electroplating Ni (~350 µm) to form fiber wires; (iii) embedding these fibers in IN718 structures fabricated by Laser DED AM technique; and (iv) post-electroplating to fill grooves and strengthen bonding. In addition, LSP treatment was performed using a Q-switched Nd:YAG laser (1064 nm, 7 ns, 850 mJ), which develops compressive microstrains (i.e., ~130 µε) around the embedded fibers. This process refined the Ni microstructure, reducing grain size from 117 µm to 93 µm (65% overlap) and increased the fiber slippage temperature from 252 °C to 305 °C. Consequently, it resulted in improved bonding strength and enhanced thermal stability of the embedded sensors.

3.2.2 Wire-arc directed energy deposition

Huang et al. [43] fabricated a smart metal beam with subsurface-embedded SGs and RTDs using a hybrid additive–subtractive manufacturing process, as shown in Fig. 8e. The fabrication steps include: (i) fabricating the host structure using WAAM with Al 5356 wire feedstock; (ii) extracting the beam from the host structure, followed by machining sensor cavities on the beam using CNC milling; (iii) attaching SGs and RTDs into the cavities; (iv) applying a ceramic protective layer to shield sensors from excessive heat; (v) metallize the surface via cold spray additive manufacturing (CSAM) using Al–Al_2O_3–Zn powder mixture to fully encapsulate the sensors. Then the embedded sensors were wired to a DAQ system for real-time monitoring and the tests showed ≤0.5% temperature error for RTDs and consistent SG strain response under three-point bending tests, which exhibits the system's functional reliability. The hybrid (WAAM, CNC and CSAM) approach provided successful embedding of sensors while maintaining structural integrity, despite reduction of 20.6% in flexural modulus and 18.9% in yield strength relative to the baseline beam. Notably, unlike prior studies that typically embedded a single sensor, this work integrated a network of sensors (2 SGs + 3 RTDs), demonstrating the feasibility of multi-sensor integration within additively manufactured metallic structures.

Likewise, in a recent work, Zhou et al. [44] fabricated a self-aware metallic smart beam with subsurface-embedded PZT sensors using a similar hybrid additive–subtractive manufacturing process. The fabrication procedure involved (see Fig. 8f): (i) building the host structure (Al-5356) via WAAM; (ii) CNC milling to extract the beam and machine 1.5 mm-deep cavities for sensor placement; (iii) embedding commercial PZT sensors (*Acellent SMLSSOP4NR*; one actuator, one receiver); (iv) applying a ceramic thermal-barrier coating for protection; and (v) encapsulating the sensors by CSAM metallization using an Al–Al_2O_3–Zn powder blend. The embedded PZTs functioned as both actuators and sensors in pitch-catch guided-wave (GW) tests under mechanical (0–100 MPa) and thermal (ambient to 100 °C) loadings. The signals showed clear stress- and temperature-dependent

changes to the applied loadings, which matched with the performance of surface-mounted PZTs. This hybrid manufacturing process enabled sensor embedding with enhanced performance, functionality, advancing the development of self-aware metallic structures with integrated SHM. Collectively, this body of work demonstrated the WAAM-dominant convergent manufacturing approach as a feasible and effective pathway for integrating functional sensors into metallic structures, achieving real-time SHM functionality.

3.3 SMS fabricated via ultrasonic additive manufacturing (UAM)

Hyer et al. [46] developed a smart pipe with embedded sensors using UAM of stainless steel (SS304). The smart heat pipe, shown in Fig. 9a, included Cu-coated fiber optic strain sensors and a Type-K TC (*Model: TJ36-CASS-116U-36, Omega Engineering*). Sensors were embedded in machined channels on the pipe wall, with larger channels left open for external sensors to validate embedded sensor data. UAM was used to weld SS304 foils over embedded sensors. When nickel-plated SS304 foils were used, bonding was improved compared to using pure SS304 foils. The embedded sensors measured temperature and strain accurately, showing good agreement with external sensors, with a temperature difference of 80–100 °C.

Zhao et al. [19] utilized the UAM of 0.15-mm-thick Al (6061 H18) foils to develop a smart device for strain measurement. The sensor system comprised a high-speed FBG strain sensor. The fabricated SMS is shown in Fig. 9b, which includes the optical microscopic image exhibiting the cross-sectional view of the embedded FBG sensor. The fabrication of this strain measuring SMS involved the following steps: (i) manufactured the substrate using Al foils through UAM; (ii) machined a cavity using a ball nose type endmill; (iii) inserted the FBG strain sensor into the cavity; (iv) resuming the UAM process to deposit additional Al foils onto the sensor embedded substrate; (v) performing machining to achieve the desired size and shape of the smart part. The embedded FBG strain sensor was fully functional and measured the phase and amplitude of different high-speed dynamic events at a rate of up to 10 kHz, with a minimum strain detection sensitivity of 2.5 με. The accuracy was confirmed through finite element analysis (FEA), offering an economical solution for monitoring dynamic strain in large-scale systems.

Ramanathan et al. [45] developed a concept for a smart nondestructive testing (NDT) device using the UAM of Al (6061-T6). The sensor comprised silver electrode coated β-phase piezoelectric polyvinylidene fluoride (PVDF) strain sensor film. As illustrated in Fig. 9c, the sensor embedding technique involved the following steps: (i) the PVDF sensor was laminated with polyimide tape (Kapton) to provide heat shielding from UAM and electrical insulation; (ii) the sensor was inserted into the machined cavity in the Al base plate and pre-compressed to ensure sufficient metal-to-metal weld strength; (iii) finally, two aluminum (6061-T6) foils were ultrasonically welded on the based plate with embedded sensor to complete the fabrication of the smart part. The fabricated part was fully functional and promising linearity under uniaxial stress. A similar approach was adopted by Khattak et al. [22] to develop comparable SMS, as shown in Fig. 9c (bottom panel).

Chilelli et al. [47] developed a smart crack detection device using the UAM of Al (6061 H18). The sensor used was an FBG strain sensor (*Moog Inc.*) coated with acrylate. The sensor operated between 1545 and 1555 nm in wavelength, with a nominal wavelength of 1550 nm, corresponding to $\pm 4000 \mu\epsilon$ inside the fiber. Fabricated tension and tensile coupon specimens embedded with FBG strain sensors are depicted in Fig. 9d. The fabrication process begins by welding a single layer of Al foil onto an Al baseplate. Then, a 0.254 mm by 0.254 mm channel was machined using a ball-type endmill, and the FBG strain sensor was inserted into the channel. The extra fiber was allowed to leave the sample, as shown in Fig. 9d. Finally, the UAM process was resumed to deposit additional aluminum layers into the embedded sensor. Finally, the smart part was machined to the required dimensions using a CNC milling machine. The embedded FBG strain sensor was capable of closely monitoring the crack growth. Moreover, early crack detection was possible, with sensors detecting cracks as small as 0.286 ± 0.033 mm at a distance of 3 mm from the crack initiation point. The embedded sensor remained fully functional even under high temperature conditions up to 300 °C. This smart crack detection device offers potential for SHM in complex systems.

Bournias-Varotsis et al. [51] also developed an SMT resistor-embedded smart part using the UAM of Al (3003-H18). The sensor type was a surface mount technology (SMT) resistor (*CRG1206 series*), and the embedding procedure is presented in Fig. 9e. First, two Al were welded ultrasonically onto a 1.5 mm thick aluminum (Al 1050-H14) base plate. Next, six Al 3003-H18 foils with pre-machined cavities were ultrasonically welded onto the substrate. The SMT resistor was then inserted into the cavity and secured with cyanoacrylate adhesive. Finally, two more Al 3003-H18 foils were placed on the substrate, covering the embedded sensor, and were bonded through UAM to complete the fabrication of SMS. Although no data was extracted from the embedded SMT resistor to verify its functionality, the sensor embedding technique could be utilized for the fabrication of additively manufactured parts with integrated three-dimensional electrical circuits.

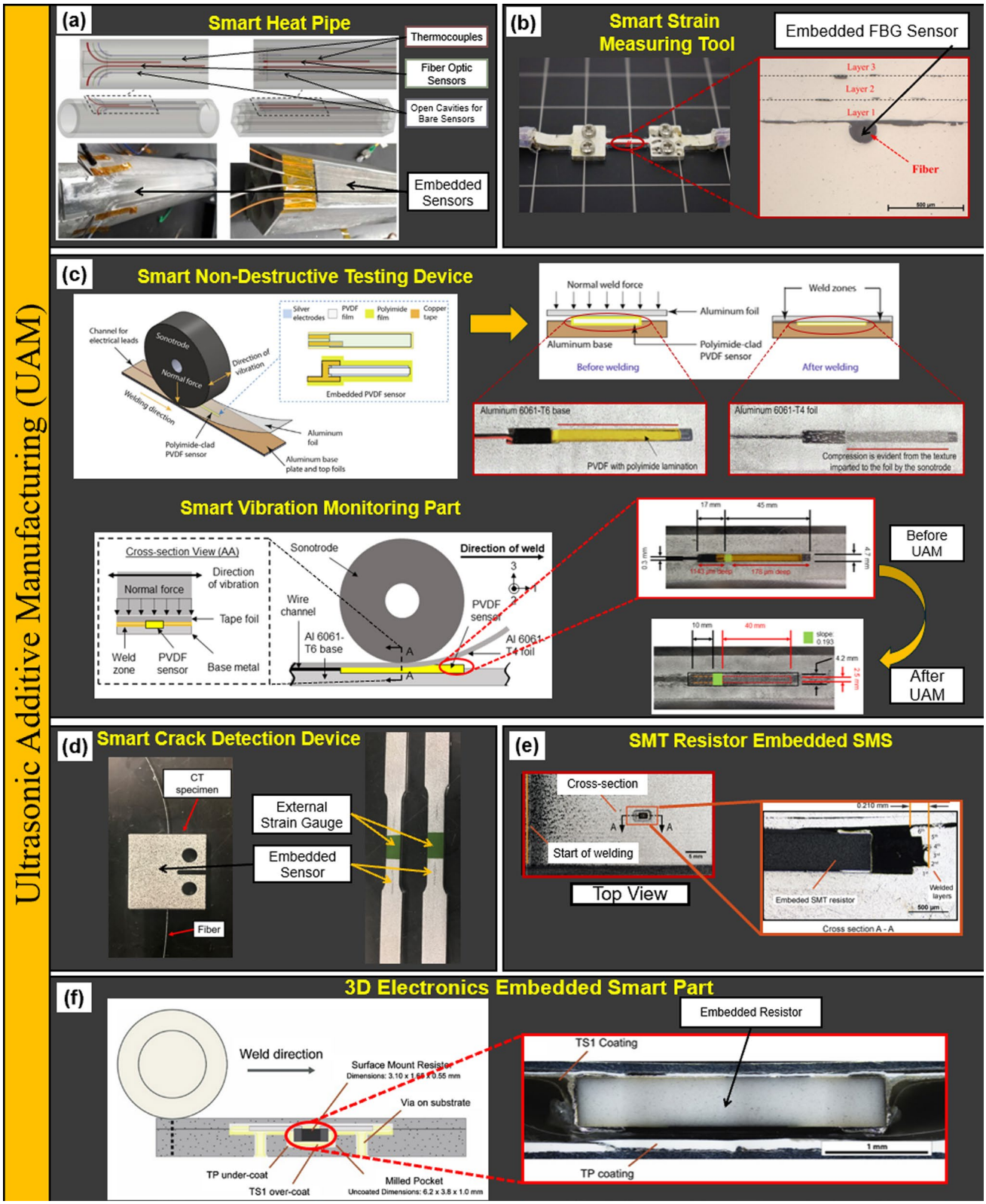

Fig. 9 SMS fabricated using UAM technique: **a** Smart heat pipe [46]; **b** Smart strain measuring tool [19]; **c** Smart non-destructive testing device (upper panel) [45] and smart vibration monitoring part (bottom panel) [22]; **d** Smart crack detection device [47]; **e** SMT resistor embedded SMS [51]; **f** 3D electronics embedded SMS [49]

Bournias-Varotsis et al. [49] fabricated a 3D electronics-embedded smart part using UAM of Al. The sensor system incorporated an SMT resistor (*Model: TE Connectivity CRG1206 series*). The sensor embedding process is shown in Fig. 9f. The process involved coating Al foils with an insulator, placing the sensor in a gap, and using conductive adhesive for thermal curing. A pocket was machined into the bottom layer to hold the sensor, with insulation layers added for thermal and electrical protection. UAM then joined the top and bottom layers. The smart part was fully functional, and the insulators successfully protected the conductive tracks and the sensor. Conductive tracks and sensors remained completely stable at temperatures as high as 60 °C, with only slight fluctuations observed at temperatures up to 100 °C.

Petrie et al. [50] adopted the same UAM approach to embed Cu, Ni, and Al-coated fiber into aluminum (Al 6061-H18) sheet. After machining a cavity, the coated fibers were placed inside, and the sheet was welded over them using UAM. While no sensors were embedded, the high-temperature survival and strong bonding suggest this method could embed fiber optic sensors for harsh environments. Similarly, Monaghan et al. [52] used UAM to embed Cu- and Al-coated optical fibers in Al 1050 with Al 3003 H18 foils. Later, Petrie et al. [48] embedded Cu-coated fiber sensors in straight and curved channels, which remained functional at temperatures up to 500 °C.

Table 4 provides a comprehensive summary of the key steps involved in sensor embedding and the fabrication of SMS as reported in the aforementioned studies, along with the associated opportunities and challenges.

3.4 Post-processing techniques for SMS

Post-processing plays a vital role in SMS fabrication to achieve the desired surface finish, dimensional precision, efficient sensing performance, etc. Various post-machining methods have been employed in the existing literature depending on the AM method and embedded sensor type (see Table 4). Common approaches include polishing, grinding, CNC milling, electrical discharge machining (EDM), and water jet cutting. For LPBF-based SMS, mechanical finishing techniques (i.e., polishing, milling, grinding, EDM) have been employed to extract the final part, eliminate surface irregularities, and expose sensing regions [16, 17, 38]. Wire EDM, in particular, has been frequently utilized for high-precision trimming or cutting, especially in sensor modules requiring electrical encapsulation [32, 41]. In UAM-based SMS, milling was often adopted to remove excess layers to fabricate SMS with TCs, PZT, and fiber optic sensors [19, 22, 45–47]. For WAAM, CNC milling prior to ceramic shielding and cold spray metallization ensured good sensor bonding with the substrate and accurate geometry for temperature and strain testing [43, 44]. Additionally, some studies have employed water-jet cutting or abrasive machining [34, 35] to achieve fine surface detailing and high dimensional accuracy. Overall, post-processing is indispensable for refining structural precision, ensuring geometric conformity, and preparing AM-fabricated SMS for subsequent functional validation (e.g., mechanical, thermal performance testing).

Besides, emerging research is actively pursuing advanced strategies to minimize or even eliminate post-processing requirements. These include in-situ surface finishing [159], remelting techniques [160], closed-loop process monitoring and adaptive control [161, 162], and multi-axis hybrid AM systems integrating machining or laser polishing [163]. Collectively, these approaches aim to achieve near-net-shape fabrication with superior surface integrity, improved dimensional precision, and significantly reduced manual intervention, thereby enhancing the overall efficiency and scalability of SMS production.

3.5 Challenges and limitations of MAM for SMS

Table 5 presents the key limitations and challenges of MAM methods for SMS fabrication, categorized across process, material, mechanical, microstructural, defects, and economic aspects. LPBF enables the fabrication of complex, high-density components with fine surface quality. Its microstructural control allows property customization, while unfused powder can be reused, minimizing material waste. Despite its advantages, LPBF remains limited in both material versatility and productivity. It is primarily compatible with a narrow range of alloys, including aluminum, magnesium, titanium, cobalt, nickel, and copper [115]. Moreover, LPBF exhibits a slower build rate due to its lower laser power (typically below 1 kW compared to EBM's 30–42 kW [121]). The reduced energy input not only extends processing time but also produces smaller melt pools, restricting the maximum feasible build size. Consequently, LPBF parts often exhibit high residual stress and complex microstructures, requiring post-processing to improve overall performance.

The EBM process operates at high beam power ranging from 30 to 42 kW [121], enabling a high production rate. The elevated powder bed temperature in EBM reduces the thermal gradient between the powders and the surrounding environment, which in turn minimizes residual stress in the fabricated part [121]. Additionally, AM parts produced by EBM exhibit a dense microstructure with enhanced mechanical performance. However, the larger beam spot size generates bigger melt pools, resulting in higher surface roughness. The deposition may also introduce sharp

Table 4 Summary of the key steps in sensor embedding and SMS fabrication, along with associated opportunities and challenges [Key steps (i-ix) are shown in Figure 3]

References	Year	*Step (i)*	*Step (ii) & (iii)*		*Step (iv)*	*Step (v)*	*Step (vi)*	*Step (vii)*	*Step (viii)*	*Step (ix)*	Resulting SMS	Opportunities	Challenges
		Sensor type	AM Method	Feedstock	Sensor embedding method	Heat shield	Metal layer restoration	AM resumption	Post processing	Data verification			
Rodrigues et al. [30]	2025	Superelastic SMA strain sensor	LPBF	AlSi10Mg	Manual insertion plus heat treatment	N/A	N/A	N/A	N/A	µCT and SEM for interface quality, SR-XRD for phase transformation, resistivity–strain testing, and FEA validation	Self-sensing metallic structure	Verified reversible phase transformation and stable resistivity–strain sensing up to 2.5% strain	Partial interfacial bonding due to limited diffusion at 300 °C and reduced adhesion quality because of the residual stress mismatch between Al and NiTi
Wang et al. [16]	2024	FBG temperature sensor	LPBF	Ti-6Al-4 V	N/A	Ti-6Al-4 V wire	Ti-6Al-4V	LPBF	Polishing	Experimental *(in situ)* and ML-predicted thermal profiles	ML-assisted sensor embedded smart structure	Machine learning-assisted miniature sized sensor with high sensitivity for *in-situ* temperature data during LPBF	Off-line sensor embedding approach
Šakalys et al. [17]	2024	SAW temperature sensor	LPBF	Stainless steel (316L)	N/A	316L cover plate	316L cover plate	LPBF	CNC milling, grinding, and electrical discharge machining	Temperature measurement	Smart injection molding tool	No visible defects such as burn mark and achieved 99.9% part density	Design challenges and signal disruptions
Ahmed et al. [18]	2024	FBG strain sensor	LPBF	Inconel 718	N/A	N/A	N/A	LPBF	N/A	Cyclic fatigue test	Sensor embedded metal part	Analyzed spectral responses and revealed relationship between the surface roughness and sensor sensitivity	Off-line sensor embedding and sensor durability issues during fatigue testing

Table 4 (continued)

References	Year	*Step (i)*	*Step (ii) & (iii)*		*Step (iv)*	*Step (v)*	*Step (vi)*	*Step (vii)*	*Step (viii)*	*Step (ix)*	Resulting SMS	Opportunities	Challenges
		Sensor type	AM Method	Feedstock	Sensor embedding method	Heat shield	Metal layer restoration	AM resumption	Post processing	Data verification			
Binder, Machnik, et al. [31]	2022	Strain gauge	LPBF	Inconel 718	Welding	N/A	N/A	LPBF	N/A	Detecting externally applied vibration	Smart vibration detector	Optimized welding parameters provided a strong bond between strain gauge and host metal matrix	Prefabricated LPBF part was used for online sensor embedding; not initially an online approach
Binder, Stapff, et al. [32]	2022	RFID transponder	LPBF	16MnCr5	N/A	Closure triangle of powder	Closure triangle of powder	LPBF	Wire EDM	Wireless data transmission	Wireless sensor-embedded gear	Sensor capable of collecting and transmitting acceleration date during gear rotation	Limited RFID transponder readout range due electromagnetic interference
Tomaz et al. [33]	2021	SAW temperature sensor	LPBF	Stainless steel (316L)	N/A	316L cover plate	316L cover plate	LPBF	N/A	Signal attenuation and thermal tests	Wireless temperature sensing device	Minimal variation between pre- and post-embedding sections, ensuring part continuity	Gaps between cover plate and main body, potentially affecting mechanical properties
Hyer et al. [34, 35]	2021	Type-K thermocouple	LPBF	Stainless steel (316)	Spot welding	SS316 sheath and MgO insulation	SS316 block	LPBF	Water jet cutting	Temperature measurement	Smart transformational challenge reactor (TCR)	Compatible with TCR components, measuring temperatures up to 500 °C	Sensor positioned on wrought plate, resulting in an off-line embedding approach
Binder et al. [36]	2020	RTD	LPBF	AlSi10Mg	Laser beam welding	Thermal paste and cold polymerizing resin	AlSi10Mg powder	LPBF	N/A	N/A	Automated sensor embedding tool	Automated sensor embedding during AM interruption, faster than manual insertion	Lower quality and stability in embedded sensor compared to manual insertion

Table 4 (continued)

References	Year	*Step (i)*	*Step (ii) & (iii)*		*Step (iv)*	*Step (v)*	*Step (vi)*	*Step (vii)*	*Step (viii)*	*Step (ix)*	Resulting SMS	Opportunities	Challenges
		Sensor type	AM Method	Feedstock	Sensor embedding method	Heat shield	Metal layer restoration	AM resumption	Post processing	Data verification			
Jung et al. [37]	2020	Type-T TC	LPBF	Inconel 718C	N/A	718C protective layer	IN718C protective layer	LPBF	N/A	Tensile test and thermal test	Smart turbine blade	Sensor embedded without any heat shielding, utilizing high thermal durability materials	Slight interfacial gap between the top and bottom AM parts
Attridge et al. [38]	2017	Type-K TC	LPBF	Inconel 718	Welding	IN718 sheath	IN718 powder	LPBF	EDM and abrasive cutting	Temperature measurement	TC-integrated turbine vane	Environmentally friendly, suitable for harsh condition applications	Off-line sensor embedding approach
Hossain et al. [39]	2016	PZT strain sensor	EBM	Ti–6Al–4 V	N/A	Alumina housing	Ti–6Al–4 V insert part	EBM	N/A	Compression test	Smart part for SHM	Enhanced lifespan of embedded sensor under harsh environments	Issues with part attachment and bonding strength due to EBM process interruption
Zhong et al. [40]	2025	Distributed optical fiber sensors	Powder DED	Inconel 718	Electroplating	Black tape (absorbing) + water (confining) layers during LSP	Electroplated Ni layers	N/A	N/A	Distributed strain measurement during LSP and thermal cycling up to 305 °C	Fiber-sensor-embedded metallic component	Improved bonding, reduced grain size (i.e., 20% refinement), and increased fiber slippage temperature from 252 °C to 305 °C	High LSP overlap can cause delamination or fiber damage, requiring precise electroplating control
Nuñez et al. [20]	2023	Type-K TC	Powder DED	Stainless steel (316L)	Hinged	316L sheath	316L sheath	Powder DED	N/A	In situ thermal test	Smart part for high-temperature measurement	Achieved high accuracy at elevated temperatures with less than 0.75% deviation from target	Embedded sensor experienced deflection due to high temperatures, a gap between sensor and host material, and porosity in AM part

Table 4 (continued)

References	Year	*Step (i)*	*Step (ii) & (iii)*		*Step (iv)*	*Step (v)*	*Step (vi)*	*Step (vii)*	*Step (viii)*	*Step (ix)*	Resulting SMS	Opportunities	Challenges
		Sensor type	AM Method	Feedstock	Sensor embedding method	Heat shield	Metal layer restoration	AM resumption	Post processing	Data verification			
Feldhausen et al. [21]	2023	N/A (Only ceramic inserts)	Powder DED	Stainless steel (316L)	N/A	Unmelted powder	Unmelted powder	Powder DED	N/A	N/A	Ceramic embedded AM part without sensor	Oblique angle metal deposition via DED protected embedded ceramic from high temperature exposure	No embedded sensor; only ceramic insert embedded without sensor
Juhasz et al. [41]	2020	Strain gauge	Powder DED	Stainless steel (300-series)	Stitch welding	Sensor plate	Laser clad	Powder DED	Milling and wire EDM	In situ data collection and cyclic loading test	Smart tensile bar	Effective thermal shielding during DED; bars provided accurate data during room-temperature tensile testing	Only one smart tensile bar with an embedded sensor survived fabrication; other sensors failed due to high-temperature exposure, resulting in low survival rate
X. Li & Prinz [42]	2003	FBG strain and temperature sensor	Powder DED	Stainless steel (316L)	N/A	Thin metallic film coating	Ni electroplating	Powder DED	N/A	Tensile, four-point bending, and oven tests	Smart part for temperature and strain monitoring	Embedded temperature sensor exhibited 100% higher sensitivity than external sensor	Sensor placed on electroplated surface with DED applied over it, rather than being embedded directly in AM part
Huang et al. [43]	2025	RTD and SG	WAAM	Al 5356	M-Bond 610 adhesive	Ceramic protective layer	CSAM	N/A	CNC milling for sensor cavities (before CSAM)	Steady-state and transient thermal tests, and three-point bending	Smart metal beam with subsurface-embedded sensors	Achieved ≤ 0.5% temperature error for RTDs and consistent strain sensing	Moderate mechanical debit (i.e., 20.6% flexural modulus and 18.9% yield strength reduction)

Table 4 (continued)

References	Year	*Step (i)*	*Step (ii) & (iii)*		*Step (iv)*	*Step (v)*	*Step (vi)*	*Step (vii)*	*Step (viii)*	*Step (ix)*	Resulting SMS	Opportunities	Challenges
		Sensor type	AM Method	Feedstock	Sensor embedding method	Heat shield	Metal layer restoration	AM resumption	Post processing	Data verification			
Zhou et al. [44]	2025	PZT sensor	WAAM	Al 5356	Loctite EA9394 Aero adhesive	Ceramic protective layer	CSAM	N/A	CNC milling for sensor cavities (before CSAM)	Static and quasi-static load tests, and thermal cycling	Self-aware metallic beam with embedded PZT sensors	Demonstrated effective guided-wave sensing under mechanical and thermal loading, proving viability for integrated SHM	Moderate reduction in stiffness and strength due to sensor cavities and single-sample testing limits statistical validation
Zhao et al. [19]	2024	FBG strain sensor	UAM	Aluminum	N/A	N/A	N/A	UAM	Milling	Static and dynamic strain tests	Smart strain measuring tool	Economical sensor embedding and dynamic strain measurement up to 10 kHz with high strain detection sensitivity	Discrepancy in dynamic strain measurement at higher frequencies (10 kHz) compared to simulation results
Khattak et al. [22]	2023	PZT strain sensor	UAM	Aluminum	Compression force	Layer of polyamide tape	N/A	UAM	Milling	Impact (i.e., axial and cantilever) and bending tests	Smart vibration monitoring part	Achieved strong mechanical coupling between sensor and host material	Part contained a sub-surface sensor, not fully embedded within the structure
Ramanathan et al. [45]	2022	PZT strain sensor	UAM	Aluminum	Compression force	Layer of polyimide tape	N/A	UAM	Milling	Tensile test	Smart non-destructive testing device	Pre-compression technique enabled strong coupling without external bonding medium	SMS featured a sub-surface rather than a fully embedded sensor

Table 4 (continued)

References	Year	*Step (i)*	*Step (ii) & (iii)*		*Step (iv)*	*Step (v)*	*Step (vi)*	*Step (vii)*	*Step (viii)*	*Step (ix)*	Resulting SMS	Opportunities	Challenges
		Sensor type	AM Method	Feedstock	Sensor embedding method	Heat shield	Metal layer restoration	AM resumption	Post processing	Data verification			
Hyer et al. [46]	2022	Fiber optic strain sensor and Type-K TC	UAM	Stainless steel (SS304)	N/A	Cu coating	Ni electroplating	UAM	Milling	Thermal test and residual strain measurement	Smart heat pipe	Enabled sensor embedding in complex structures (pipes, hexagonal blocks) for real-time temperature and strain data	Observed gaps and porosity at the interfaces of the welded sheets
Chilelli et al. [47]	2019	FBG strain sensor	UAM	Aluminum	N/A	Acrylate coating	N/A	UAM	Milling	Crack detection and high-temperature strain measurement	Smart crack detection device	SMS capable of detecting cracks at high temperatures up to 300 °C	Embedded sensor did not survive temperatures exceeding 300 °C
Petrie et al. [48]	2019	Optical fiber temperature sensor	UAM	Aluminum	N/A	Cu or Ni coating	N/A	UAM	N/A	High-temperature test	Sensor embedded channel	Sensors can be embedded into curved channels for measuring radial dimensional change	Poor bonding of the sensor with the host metal matrix in some cases
Bournias-Varotsis et al. [49]	2019	SMT resistor	UAM	Aluminum	Conductive adhesive	Different insulations	N/A	UAM	N/A	Temperature stability test	3D electronics embedded SMS	Insulators protected sensor from UAM high temperatures, ensuring stability up to 60 °C	Significant unwelded area and gaps around embedded sensor
Petrie et al. [50]	2019	Fiber	UAM	Aluminum (Al 6061-H18)	Compression force	Cu, Ni, and Al coating	N/A	UAM	N/A	N/A	Fiber optical sensor embedded metal part	High survivability and strong bonding of embedded fiber suitable for harsh environments	Fabricated part did not contain an embedded sensor; instead, fiber was embedded with significant deformation at the area

Table 4 (continued)

References	Year	*Step (i)*	*Step (ii) & (iii)*		*Step (iv)*	*Step (v)*	*Step (vi)*	*Step (vii)*	*Step (viii)*	*Step (ix)*	Resulting SMS	Opportunities	Challenges
		Sensor type	AM Method	Feedstock	Sensor embedding method	Heat shield	Metal layer restoration	AM resumption	Post processing	Data verification			
Bournias-Varotsis et al. [51]	2018	SMT resistor	UAM	Aluminum (3003-H18)	Cyanoacrylate adhesive	N/A	N/A	UAM	N/A	N/A	SMT resistor-embedded SMS	Developed predictive model for sensor location, size, and tolerance based on experimental data	No data collected from embedded SMT resistor to verify functionality; long gaps around embedded sensor
Monaghan et al. [52]	2015	Fiber optic	UAM	Aluminum (Al 3003 H18)	N/A	Al and Cu coating	N/A	UAM	N/A	N/A	Optical fiber embedded metal part	Strong bonding of fiber to welded sheets with full functionality, expanding SHM potential in new applications	Part contained an embedded fiber rather than a sensor

[Key steps (i-ix) are shown in Fig. 3]

Table 5 Key challenges and limitations of MAM methods for SMS across various categories

Category	LPBF	EBM	Powder DED	Wire-arc DED	UAM
Process	Narrow process window; prone to porosity; and lack-of-fusion from sub-optimal laser parameters [115]	High beam energy causes rough surface, while dedicated vacuum requirement limits productivity [121]	Complex melt-pool dynamics, thermal cycling, and nozzle design factors contribute to residual stress, distortion, and low powder utilization efficiency [136, 164]	High heat input and arc instability lead to distortion and uneven bead geometry [168]	Sensitive to amplitude and pressure, along with insufficient energy input, often results in weak interlayer bonding between foils [151]
Material	Oxidation, irregular powder size, and poor flowability reduce interparticle bonding and overall part density [121]	Preheating reduces stress but promotes grain coarsening [115]	Powder oxidation, irregular powder shape, and flow inconsistency lead to porosity formation[114]	Wire oxidation and contamination create inclusions and fusion defects [167]	Hard metals (i.e., Ti, steel) show poor plastic flow and bonding due to high hardness [149]
Mechanical	High residual stresses and distortion from rapid thermal cycles require post-processing treatments [121]	Surface roughness and notch formation reduce fatigue strength [121]	Large grain size and anisotropy decrease tensile and fatigue strength [139]	Residual stresses and warping require stress-relief treatments [166]	Weak interfacial strength and oxide retention lower joint reliability [154]
Microstructural	Fine anisotropic grains results in non-uniform mechanical properties [115]	Columnar β grains and anisotropy arise from directional solidification [115]	Coarse dendritic structure lowers fatigue resistance [139]	Coarse columnar grains and anisotropy reduce toughness [168]	Thin bond zones and limited recrystallization lead to anisotropy [156]
Defects	Porosity, keyholes, and lack of fusion defects arise from unstable laser melt pools [115]	Rough surfaces, unmelted particles, and minor porosity [121]	Porosity, cracks, and spatter result from poor powder-laser interaction [114]	Porosity, cracking, and lack of fusion due to arc instability [167]	Delamination, resonance cracking, and voids at foil interfaces [149]
Economic / Scalability	High energy cost and limited alloy options restrict scalability [115]	Expensive vacuum system cost and low production throughput [121]	Low dimensional accuracy and high post-processing cost [136]	Poor surface finish and extensive requirement reduce overall cost efficiency [168]	Low deposition rate, limited material range, and complex post-processing constrain industrial scalability [150]

notches, increasing susceptibility to fatigue cracking and reducing fatigue life. Moreover, EBM is energy-intensive, with high equipment and maintenance costs, and requires a dedicated vacuum environment to prevent electron scattering. Its application is further limited to metallic materials, whereas LPBF can process metals, ceramics, and polymers.

Laser-powder DED enables the fabrication of functionally graded materials by integrating multiple compositions within a single build [114]. This capability is particularly beneficial for applications demanding spatially varied properties or the incorporation of dissimilar materials to achieve specific functionalities. Moreover, owing to its multi-axis capabilities, L-DED is particularly well suited for component repair and remanufacturing, enabling precise material deposition [136]. Additional advantages include support for large build volumes, high deposition rates, and minimal post-processing to achieve the desired geometric precision and dimensional accuracy [135]. Despite these benefits, L-DED presents several challenges. The dynamic thermal environment during deposition induces significant residual stresses due to steep temperature gradients and cyclic heating–cooling effects [139]. Parts fabricated via L-DED often exhibit rough surface finishes, and material utilization efficiency is relatively low (50–80%) because not all powder is fully melted during deposition [164]. Moreover, maintaining an inert atmosphere requires substantial argon or nitrogen consumption, increasing operational costs.

Wire DED (i.e. WAAM) offers nearly 100% material utilization and operates without requiring a dedicated vacuum environment, while also enabling multi-axis robotic capabilities for large-scale part manufacturing [165]. However, it still faces several challenges related to heat input control and process stability. Excessive heat accumulation often causes distortion, residual stresses, cracking, porosity, surface waviness, and warpage, deteriorating dimensional accuracy and mechanical properties [166]. The non-uniform temperature distribution during multilayer deposition leads to thermal gradients and grain coarsening, which reduce toughness and induce anisotropy in built parts [167]. In addition, process control remains difficult since parameters such as wire-feed speed, travel speed, and arc current strongly influence melt-pool dynamics, defect formation, and interlayer bonding [166]. Furthermore, in WAAM, achieving consistent microstructure and surface finish across large geometries is limited by arc instability and environmental disturbances [168]. WAAM also suffers from residual stress, oxidation, and

limited precision compared to the powder-based AM methods, and it needs extensive post-processing (i.e., subtractive machining) to meet geometric accuracy requirements [167, 168].

UAM produces components with minimal residual stress through a solid-state bonding mechanism [151], effectively avoiding the thermal gradients typical of fusion-based methods [150]. The process enables joining of dissimilar materials, making it suitable for multifunctional applications, while its low-temperature operation preserves base-material properties and ensures environmental sustainability by eliminating harmful byproducts [149]. However, UAM remains limited by incompatibility with hard steels and nickel-based alloys, as well as by restricted processing speed, build volume, and layer thickness [154, 156]. Bonding inconsistencies may also occur, and its relatively small production scale limits applicability to large-scale manufacturing.

Despite the limitations of MAM methods listed in Table 5, they offer significant advantages over traditional subtractive approaches for smart metallic structure (SMS) fabrication. MAM enables highly efficient material utilization by minimizing waste and eliminating the need for extensive machining, while offering unparalleled design flexibility to produce complex geometries, internal channels, and lattice structures. The capability to deposit multi-materials within a single build allows for compositionally graded and site-specific property tailoring. Furthermore, MAM facilitates the direct embedding of sensors, electronic components, or reinforcements during fabrication, enabling multifunctional, self-sensing, or self-healing structures. From a sustainability perspective, MAM processes are inherently more environmentally friendly than conventional manufacturing, as they reduce raw material waste, machining fluids, and energy consumption associated with extensive subtractive operations. In addition, their tool-free nature supports rapid prototyping and on-demand manufacturing, drastically reducing lead time and cost. Finally, the ability to locally repair or rebuild damaged regions enhances the service life and maintainability of critical components, positioning MAM as a transformative pathway for developing intelligent, resource-efficient, and high-performance smart metallic systems.

4 Technological advantages, challenges, and emerging directions of SMS

4.1 Technological advantages

Based on the extensive review of current literature, the primary technological advantages of additively manufactured SMS can be identified and summarized as follows:

Fig. 10 Challenges and limitations in SMS fabrication: **a** Sensor packaging with large footprint ceramic shielding [39]; **b** Poor interfacial adhesion strength between the heat shield and metal layer [21]; **c** Air gap and unwelded regions [49, 51]; **d** Undesired deflection, porosity, and residual stress [20]

- *Design flexibility:* MAM techniques allow for the fabrication of complex geometries that are often challenging to achieve using traditional manufacturing methods. This flexibility is particularly beneficial for SMS, where functional sensors can be embedded within intricate structures.
- *Precision and customization:* AM facilitates sensor placement within complex geometries, enabling highly customized designs tailored for specific applications.
- *Sensor integration during fabrication:* Sensors can be embedded directly into the structure during the manufacturing process.
- *Multi-material capability:* AM offers the capability to fine-tune material properties with tailored microstructure with multiple materials for demanding environmental conditions. It could be particularly useful for creating functional gradient layers to enhance sensor performance.
- *Material efficiency:* MAM processes often lead to less material waste compared to subtractive approaches.
- *Real-time monitoring:* The embedded sensors enable real-time monitoring of structural health, allowing for predictive maintenance and improved safety in critical applications.

4.2 Current limitations and challenges

Despite the abovementioned advantages, several critical limitations hinder the large-scale deployment of additively manufactured SMS. Based on the literature review, the following key process-related hurdles have been identified:

- *Sensor density and AM process of interest:* Most existing studies are primarily limited to single sensors (e.g., temperature, strain) and do not involve networks of sensors capable of mapping 3D measurement fields, such as spatial strain and temperature distribution. Additionally, the studies have focused on only a limited number of MAM methods, as outlined in Section 3.
- *Sensor packaging:* Ceramic heat shields have been employed to protect the sensors from thermal damage during the subsequent metal deposition step. However, given that the heat shield dimensions (footprint) are significantly larger than the underlying sensor (see Fig. 10a), this approach would result in notable parasitic effects within the AM build, thereby potentially

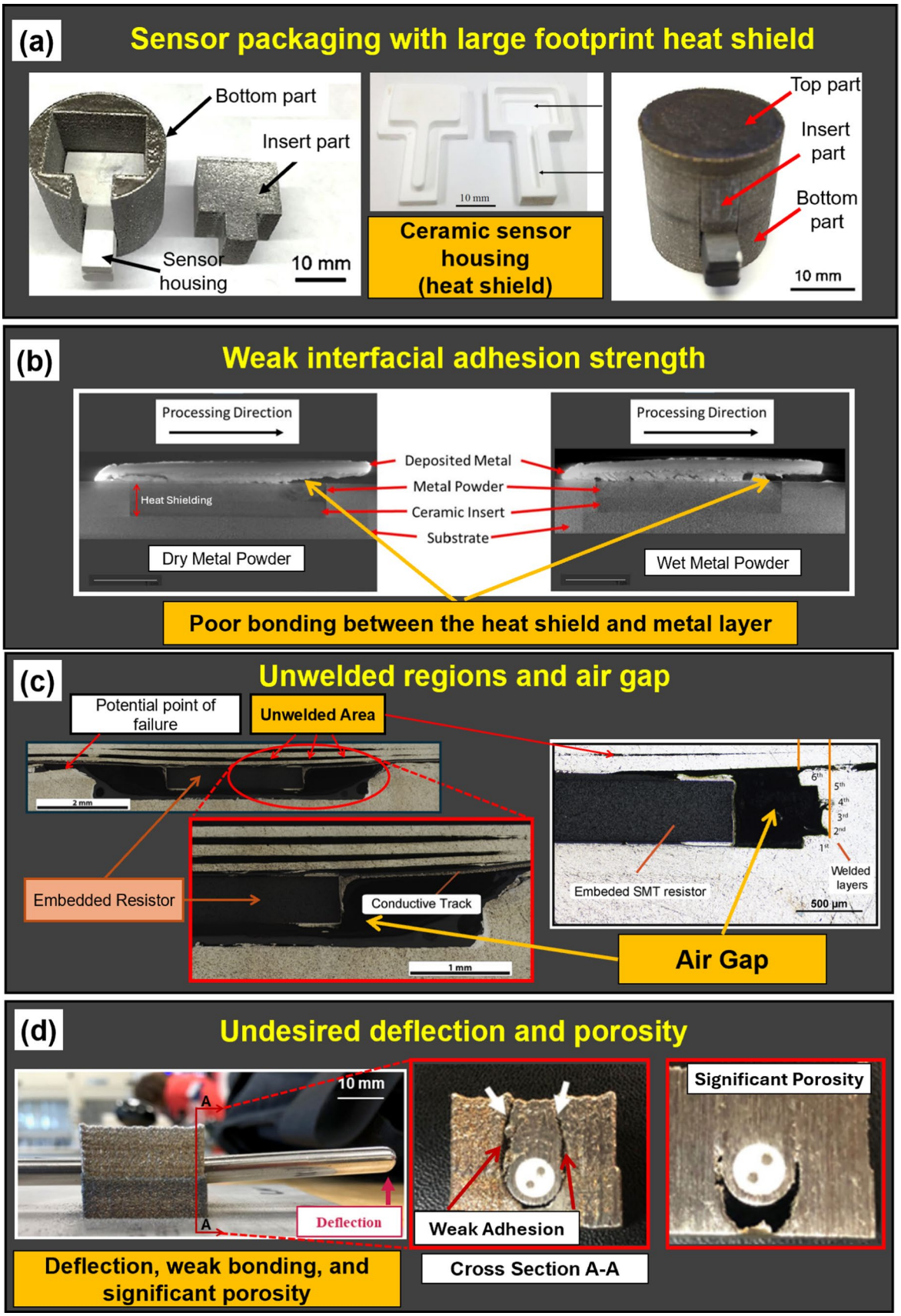

compromising the intrinsic mechanical properties of the host structure.

- *Interfacial adhesion strength:* Resuming AM deposition over the ceramic shield or powder stack without any surface treatment often leads to poor bonding between the heat shield and metal layers (Fig. 10b). Such weakly bonded layers around the embedded sensor can damage the sensor, reduce the expected operational lifetime of the AM part, and compromise the sensor's signal fidelity.
- *Unwelded (non-consolidated) areas:* Imperfect bonding between the AM base material and the sensor region/over-layer interface can result in unwelded or partially bonded areas. These regions mainly arise due to insufficient heat transfer, misalignment, or inconsistent deposition during the manufacturing process. Defects, such as non-consolidated regions and air gaps (voids) within the build (see Fig. 10c), can compromise mechanical integrity, reduce load transfer efficiency, and may act as initiation points for crack propagation under mechanical or thermal loading.
- *Residual stress:* High-temperature nature of MAM techniques often induces thermal residual stresses within the build, which can lead to distortion of the structure or sensors as well as large voids and porosity between the AM base and the sensor region (see Fig. 10c–d).
- *Scalability:* While MAM excels at producing SMS for small and complex parts, scaling these structures to larger sizes while maintaining sensor functionality remains a challenge.
- Besides these process-specific challenges, AM of SMS often requires post-processing steps (e.g., surface finishing, additional assembly, etc.) to achieve a near-net-shape product, which adds complexity, increases production time, and raises costs.

4.3 Emerging directions

The future advancement of SMS will be driven by the convergence of advanced AM technologies, intelligent process control, and data-driven manufacturing. Although substantial progress has been achieved in material deposition, microstructural optimization, and embedded sensing, three particularly promising directions stand out: (i) multi-material additive manufacturing (MMAM); (ii) self-healing and self-adaptive metallic systems; and (iii) artificial-intelligence (AI)-driven predictive manufacturing.

Multi-material additive manufacturing (MMAM) offers opportunities to fabricate SMS with spatially tailored properties, combining structural, functional, and sensing capabilities within a single component [169]. Existing MAM platforms have been adapted for multi-material fabrication through approaches such as sequential or multi powder feeding [170], coaxial wire blending, [171]. These techniques allow the controlled deposition of dissimilar metals and alloys to form functionally graded structures with smooth transitions between load-bearing and sensor-embedded regions, thereby enhancing both mechanical performance and functional integration. Recent advancements in MMAM focus on embedding sensing functionalities within metallic matrices to realize smart and self-aware systems [43, 44]. Hybrid WAAM and CS processes have demonstrated co-deposition of conductive, dielectric, or piezoelectric phases for in situ strain and temperature sensing, while CS is being explored to integrate triboelectric layers for self-powered sensing [172–174]. Despite these promising developments, key challenges remain, including interfacial integrity between dissimilar materials, process repeatability, limited spatial resolution for fine-scale integration, and the absence of predictive design frameworks. Overcoming these limitations will be essential to achieving reliable, scalable, and fully integrated MMAM-based SMS.

The development of self-healing and self-adaptive metallic systems represents a promising direction in advancing SMS, aiming to enhance their lifetime, reliability, and resilience under demanding service conditions. Recent progress in shape-memory alloys (SMA), reversible phase-transforming materials, and microencapsulated healing agents has demonstrated the potential to restore structural integrity and functional performance after damage [175]. Beyond self-repair, self-adaptive metallic systems integrate embedded sensors, functional coatings, and active materials that enable real-time adjustment of stiffness, damping, or thermal conductivity in response to dynamic operating environments [176, 177]. The fusion of self-healing and self-adaptive functionalities offers a promising pathway toward intelligent, responsive metallic structures capable of autonomous performance optimization.

The integration of machine learning (ML) and AI into SMS manufacturing marks a transformative step toward predictive, self-optimizing metallic systems. By leveraging data from in-situ sensors, ML algorithms can detect anomalies in real time, enabling early defect prediction and process correction. Supervised learning models are being trained to correlate process parameters (e.g., laser power, feed rate, deposition temperature) with resulting microstructural and mechanical properties, enhancing process reliability and repeatability [178, 179]. Meanwhile, reinforcement learning and digital twin frameworks are enabling adaptive control, where systems dynamically adjust deposition strategies to minimize porosity, distortion, and residual stress [180, 181]. These AI-driven approaches not only improve fabrication quality but also significantly increase throughput—an essential step toward the commercialization of SMS.

As computational power and sensor integration continue to advance, the synergy between data-driven modeling and AM may enable the fabrication of next-generation smart metallic systems with unparalleled precision and functionality.

5 Conclusions and outlook

This review highlighted the pioneering efforts in the field of AM of SMS, focusing on early advancements in process and material development, process optimization, and integration of sensing capabilities within the metal components. The reviewed literature has elucidated critical aspects of various MAM techniques while contributing to the advancement of intelligent metal-based systems. Based on this study, the following conclusions and future trends can be drawn:

1. Various MAM methods have been utilized in the fabrication of SMS, with particular interest in methods that enable online sensor embedding for passive sensing, facilitating real-time structural monitoring. While several MAM methods have already been applied, other MAM techniques (e.g., AFSD, SLS, binder jet, laser-wire DED) remain untested for the SMS fabrication, presenting opportunities for further innovation in this field.
2. Although various types of feedstock metals have been used to create SMS, many material systems remain unexplored in the AM of SMS (see Table 3). Moreover, multi-material AM and self-healing strategies offer complementary pathways for developing multifunctional SMS, representing a promising direction for future research.
3. Sensor miniaturization is also critical for reducing the footprint of embedded sensors and minimizing their impact on the mechanical properties of the host structure. Smaller sensors can be more easily integrated into complex geometries, enabling the development of distributed sensor networks within metal components rather than relying on single sensing element. This feature can enhance spatial resolution of sensor data, enabling more precise monitoring across the structure. In this context, beyond the use of commercial off-the-shelf sensors, the design, development, and direct printing of sensors from functional materials (e.g., metal inks, powders) onto the host structure present promising avenues for future advancements.
4. Sensor packaging and heat shielding are essential for maintaining the structural integrity of embedded sensors and preserving signal fidelity. In this context, conformal sensor packaging approaches, such as flexible printed circuit packaging offer adaptable solutions that conform to complex geometries and provide both mechanical protection and thermal insulation with a minimal footprint, ensuring reliable sensor operation in demanding environments.
5. Adhesion/bond strength at the metal-sensor-heat shield interfaces are crucial for the seamless resumption of the MAM process, ensuring both sensor fidelity and mechanical integrity of the resulting smart structure with minimal parasitic effects. Future research should focus on developing tailored surface treatments, advanced bonding techniques, and material compatibility strategies to improve adhesion and overall structural performance in SMS fabrication.
6. Regarding unwelded or non-consolidated regions in MAM, future research should prioritize advanced interfacial engineering strategies to mitigate these defects. Specifically, this includes optimizing thermal management during deposition, implementing real-time process monitoring to detect bonding inconsistencies, and developing hybrid post-processing techniques (e.g., hot isostatic pressing, laser reflow) to enhance metallurgical bonding for interfacial integrity. These strategies are also expected to help mitigate tensile residual stress, thereby improving the overall structural reliability and performance of SMS.
7. While MAM demonstrates strong potential for fabricating small and complex components, extending these capabilities to large-scale structures without compromising sensor functionality or structural integrity requires further research. In addition, the reliance on post-processing steps—such as surface finishing and secondary assembly—adds complexity, time, and cost. Future efforts should focus on process optimization, modular design strategies, and integrated manufacturing workflows that minimize post-processing requirements and enable scalable, cost-effective production of multifunctional SMS.
8. In addition to the above-mentioned avenues, simulation-guided and AI-assisted process optimization, sensor network design, and self-diagnostic are vital for optimizing sensor placement and achieving accurate field measurements (e.g., strain, temperature) from a limited number of embedded sensors. Machine learning algorithms can further enhance this process by predicting stress and thermal gradients, optimizing configurations, and improving data fusion for real-time monitoring. Ultimately, these approaches can enable efficient data acquisition and structural assessment while preserving the mechanical integrity and performance of SMS under demanding conditions.

Acknowledgements This work was funded under the Defense Advanced Research Projects Agency (DARPA)- SENSE: Structural

Evaluation through Non-contact Sensor Embedding Program. The authors wish to acknowledge DARPA for funding this work, as well as for the valuable guidance and feedback.

Author contributions All authors contributed to the writing and reviewing of the manuscript.

Funding Defense Advanced Research Projects Agency (DARPA), HR00112490367.

Data availability No datasets were generated or analysed during the current study.

Declarations

Conflict of interest The authors declare no competing interests.

References

1. Senesky DG, Jamshidi B, Cheng KB, Pisano AP (2009) Harsh environment silicon carbide sensors for health and performance monitoring of aerospace systems: a review. IEEE Sens J 9:1472–1478. https://doi.org/10.1109/JSEN.2009.2026996
2. BM Kannan, P Solainayagi, H Azath, S Murugan, C Srinivasan, (2023) Secure Communication in IoT-enabled Embedded Systems for Military Applications using Encryption, In: 2023 2nd Int. Conf. Edge Comput. Appl. ICECAA, 2023: pp. 1385–1389. https://doi.org/10.1109/ICECAA58104.2023.10212400.
3. Pourrahmani H, Yavarinasab A, Zahedi R, Gharehghani A, Mohammadi MH, Bastani P, Van herle J (2022) The applications of Internet of Things in the automotive industry: a review of the batteries, fuel cells, and engines. Internet Things 19:100579. https://doi.org/10.1016/j.iot.2022.100579
4. Ferreira PM, Machado MA, Carvalho MS, Vidal C (2022) Embedded sensors for structural health monitoring: methodologies and applications review. Sensors 22:8320. https://doi.org/10.3390/s22218320
5. Zaman S, Leyva A, Hassan MS, Valladolid A, Herrera NE, Gomez SG, Mahmud MS, Tucker D, Haynes C, Lin Y (2023) Implementation of smart materials for actuation of traditional valve technology for hybrid energy systems. Actuators 12:131. https://doi.org/10.3390/act12030131
6. Petrie CM, Leonard DN, Yang Y, Trammell MP, Jolly BC, Terrani KA (2019) Embedment of sensors in ceramic structures, Oak Ridge National Laboratory (ORNL), Oak Ridge. TN (United States). https://doi.org/10.2172/1564172
7. Stano G, Ovy SMAI, Edwards JR, Cianchetti M, Percoco G, Tadesse Y (2023) One-shot additive manufacturing of robotic finger with embedded sensing and actuation. Int J Adv Manuf Technol 124:467–485. https://doi.org/10.1007/s00170-022-10556-x
8. Qiu K, Zhao Z, Haghiashtiani G, Guo S-Z, He M, Su R, Zhu Z, Bhuiyan DB, Murugan P, Meng F, Park SH, Chu C-C, Ogle BM, Saltzman DA, Konety BR, Sweet RM, McAlpine MC (2018) 3D printed organ models with physical properties of tissue and integrated sensors. Adv Mater Technol 3:1700235. https://doi.org/10.1002/admt.201700235
9. Hu Y, Li Y, Yan D, Jiao Z, Yuan D, Qin C, Li Y (2024) Strain transfer of fiber Bragg grating sensors in fiber-reinforced polymer composites with different fiber orientations and temperatures. Measurement 225:114005. https://doi.org/10.1016/j.measurement.2023.114005
10. Ngiejungbwen LA, Hamdaoui H, Chen M-Y (2024) Polymer optical fiber and fiber Bragg grating sensors for biomedical engineering applications: a comprehensive review. Opt Laser Technol 170:110187. https://doi.org/10.1016/j.optlastec.2023.110187
11. Zhang F, Gong L, Wang F, Zhou H, He W, Huang Z, Peng X, Zhou H (2023) Embedded Pt-PVDF sensor without compromising mechanical properties of GFRP for on-line sensing. Thin-Walled Struct 187:110702. https://doi.org/10.1016/j.tws.2023.110702
12. Barragán J, Kell A, Liu X, Shin S, Mandache C, Djokic D, Bennett D, Houlahan K, Genest M, Lessard BH, Paquet C (2025) Next-generation embedded printed sensors for near-field monitoring of high-performance composites. Adv Eng Mater. https://doi.org/10.1002/adem.202401332
13. Wang Z, Yang L, Zhang S, Hu W, Hu C, Yang B (2024) Damage detection of FRP structures using the electrical resistance response of MWCNTs networks in a PDMS film substrate. Sens Actuators A Phys 366:114996. https://doi.org/10.1016/j.sna.2023.114996
14. Pan'kov AA (2021) Diagnostics of gradient strains field in polymer composite material with built-in fiber optic piezosensor. IOP Conf Ser Mater Sci Eng 1029:012063. https://doi.org/10.1088/1757-899X/1029/1/012063
15. Nagulapally P, Shamsuddoha M, Herath T, Djukic L, Prusty GB (2023) Mechanical and optical performance evaluations of embedded polyimide and PEEK coated distributed optical sensors in glass fibre reinforced composites with vinyl ester resin systems. J Compos Mater 57:1707–1728. https://doi.org/10.1177/00219983231160866
16. Wang R, Wang R, Dou C, Yang S, Gnanasambandam R, Wang A, Kong Z (James) (2024) Sub-surface thermal measurement in additive manufacturing via machine learning-enabled high-resolution fiber optic sensing. Nat Commun 15:7568. https://doi.org/10.1038/s41467-024-51235-7
17. Šakalys R, O'Hara C, Kariminejad M, Weinert A, Kadivar M, Zluhan B, McAfee M, McGranaghan G, Tormey D, Raghavendra R (2024) Embedding a surface acoustic wave sensor and venting into a metal additively manufactured injection mould tool for targeted temperature monitoring. Int J Adv Manuf Technol 130:5627–5640. https://doi.org/10.1007/s00170-023-12932-7
18. Ahmed F, Forhad MS, Porag MH (2024) Spectral behavior of fiber Bragg gratings during embedding in 3D-printed metal tensile coupons and cyclic loading. Sensors 24:3919. https://doi.org/10.3390/s24123919
19. Zhao J, Dong W, Hinds T, Li Y, Splain Z, Zhong S, Wang Q, Bajaj N, To A, Ahmed M, Petrie CM, Chen KP (2024) Embedded fiber Bragg grating (FBG) sensors fabricated by ultrasonic additive manufacturing for high-frequency dynamic strain measurements. IEEE Sens J 24:2853–2862. https://doi.org/10.1109/JSEN.2023.3343604
20. Nuñez L, Sabharwall P, van Rooyen IJ (2023) In situ embedment of type K sheathed thermocouples with directed energy deposition. Int J Adv Manuf Technol 127:3611–3623. https://doi.org/10.1007/s00170-023-11624-6
21. Feldhausen T, Yelamanchi B, Gomez A, Du Plessis A, Heinrich L, Saleeby K, Fillingim K, Post B, Love L, Cortes P, MacDonald E (2023) Embedding ceramic components in metal structures with hybrid directed energy deposition. Int J Adv Manuf Technol 125:4425–4433. https://doi.org/10.1007/s00170-023-10812-8
22. Khattak MM, Headings LM, Dapino MJ (2023) Dynamic response of a polyvinylidene fluoride (PVDF) sensor embedded in a metal structure using ultrasonic additive manufacturing. Actuators 12:428. https://doi.org/10.3390/act12110428
23. Ompal VM, Mishra A, Kumar, (2022) FPGA integrated IEEE 802.15.4 ZigBee wireless sensor nodes performance for industrial plant monitoring and automation. Nucl Eng Technol 54:2444–2452. https://doi.org/10.1016/j.net.2022.01.011

24. Xu X, Ran B, Jiang N, Xu L, Huan P, Zhang X, Li Z (2024) A systematic review of ultrasonic techniques for defects detection in construction and building materials. Measurement 226:114181. https://doi.org/10.1016/j.measurement.2024.114181
25. Arévalo LA, Pereira JC, Amorebieta J, Villatoro J, Huertos F (2024) Embedding of fiber optic sensors in metal parts by laser welding and additive manufacturing: a review. IEEE Sens J 24:13743–13757. https://doi.org/10.1109/JSEN.2024.3375773
26. Armstrong M, Mehrabi H, Naveed N (2022) An overview of modern metal additive manufacturing technology. J Manuf Process 84:1001–1029. https://doi.org/10.1016/j.jmapro.2022.10.060
27. Structural Evaluation through Non-contact Sensor Embedding, (n.d.). https://www.darpa.mil/program/structural-evaluation-through-non-contact-sensor-embedding (accessed October 23, 2024).
28. Hassan MS, Zaman S, Dantzler JZR, Leyva DH, Mahmud MS, Ramirez JM, Gomez SG, Lin Y (2023) 3D printed integrated sensors: from fabrication to applications—a review. Nanomaterials 13:3148. https://doi.org/10.3390/nano13243148
29. Resendes T, Freitas Rodrigues P, Cruz F, Gatões D, Santos VM, Ramos AS, Vieira MT (2025) Advanced medical monitoring: 3D printed prosthetics with integrated strain sensor. Prog Addit Manuf 10:219–229. https://doi.org/10.1007/s40964-024-00615-y
30. Freitas Rodrigues P, Cacho L, Gatões D, Alves B, Neto MA, dos S. Paula A, Fernandes FMB, Ramos AS, Vieira MT (2025) Embedded NiTi strain sensors in additively manufactured AlSi10Mg: computational and experimental insights into phase transformation and sensing performance. Results Eng 28:107395. https://doi.org/10.1016/j.rineng.2025.107395
31. M Binder, A Machnik, M Bosch, K Kreitz, G Schlick, C Seidel, (2022) In-situ Integration of Weldable Strain Gauges in Components Manufactured by Laser-Based Powder Bed Fusion,. https://hdl.handle.net/2152/117452 (accessed August 23, 2024).
32. Binder M, Stapff V, Heinig A, Schmitt M, Seidel C, Reinhart G (2022) Additive manufacturing of a passive, sensor-monitored 16MnCr5 steel gear incorporating a wireless signal transmission system. Procedia CIRP 107:505–510. https://doi.org/10.1016/j.procir.2022.05.016
33. Tomaz I, Uí Mhurchadha SM, Marques S, Quinn P, Funke H, Birkholz F, Zietzschmann S, Raghavendra R (2021) The development of a smart additively manufactured part with an embedded surface acoustic wave sensor. Addit Manuf Lett 1:100004. https://doi.org/10.1016/j.addlet.2021.100004
34. Hyer HC, Carver K, List FA III, Petrie CM (2021) Embedding sensors in 3D printed metal structures, oak ridge national laboratory (ORNL), Oak Ridge. TN (United States). https://doi.org/10.2172/1818670
35. Hyer HC, Carver K, List FAL Iii, Petrie CM (2023) Embedding thermocouples in SS316 with laser powder bed fusion*. Smart Mater Struct 32:02LT01. https://doi.org/10.1088/1361-665X/acae4c
36. Binder M, Dirnhofer C, Kindermann P, Horn M, Schmitt M, Anstaett C, Schlick G, Seidel C, Reinhart G (2020) Procedure and validation of the implementation of automated sensor integration kinematics in an LPBF system. Procedia CIRP 93:1304–1309. https://doi.org/10.1016/j.procir.2020.04.090
37. Jung ID, Lee MS, Lee J, Sung H, Choe J, Son HJ, Yun J, Kim K, Kim M, Lee SW, Yang S, Moon SK, Kim KT, Yu J-H (2020) Embedding sensors using selective laser melting for self-cognitive metal parts. Addit Manuf 33:101151. https://doi.org/10.1016/j.addma.2020.101151
38. Attridge P, Bajekal S, Klecka M, Wu X, Savulak S, Viens D, Carey M, Miano J, Rioux W, Zacchio J, Dunst R, Straub D, Mantese J (2017) Additively manufactured IN718 components with wirelessly powered and interrogated embedded sensing, united technologies research Center, East Hartford. CT (United States). https://doi.org/10.2172/1369567
39. Hossain MS, Gonzalez JA, Hernandez RM, Shuvo MAI, Mireles J, Choudhuri A, Lin Y, Wicker RB (2016) Fabrication of smart parts using powder bed fusion additive manufacturing technology. Addit Manuf 10:58–66. https://doi.org/10.1016/j.addma.2016.01.001
40. Zhong S, Zhao K, Nguyen DS, Zhu Q, Zou R, Wu Z, Wang Q, Zhang G, Ma G, Li Y, Zaghloul MAS, To AC, Lu Y, Chen KP (2025) Improving high temperature resilience of fiber sensor embedded smart components through laser shock peening. Opt Express 33:16003–16013. https://doi.org/10.1364/OE.549584
41. Juhasz M, Tiedemann R, Dumstorff G, Walker J, Plessis AD, Conner B, Lang W, MacDonald E (2020) Hybrid directed energy deposition for fabricating metal structures with embedded sensors. Addit Manuf 35:101397. https://doi.org/10.1016/j.addma.2020.101397
42. Li X, Prinz F (2003) Metal embedded fiber bragg grating sensors in layered manufacturing. J Manuf Sci Eng 125:577–585. https://doi.org/10.1115/1.1581889
43. S Huang, J Ren, P Zhou, S Rahman, K Young, SS Rahman, S Mishra, J Samuel, F Kopsaftopoulos, S Akin, (2025) A Multifunctional Smart Metal Beam with Sub-Surface Embedded Sensors for Real-Time Structural Health Monitoring, Struct. Health Monit. 2025. https://doi.org/10.12783/shm2025/37491.
44. P Zhou, J Ren, JS Schure, S Huang, S Rahman, S Mishra, J Samuel, S Akin, F Kopsaftopoulos (2025) Embedded Piezoelectric Sensing for Metallic Components: A Novel SHM Architecture for Self-Aware Structures, Struct. Health Monit. 2025. https://doi.org/10.12783/shm2025/37301.
45. Ramanathan AK, Gingerich MB, Headings LM, Dapino MJ (2022) Metal structures embedded with piezoelectric PVDF sensors using ultrasonic additive manufacturing. Manuf Lett 31:96–100. https://doi.org/10.1016/j.mfglet.2021.08.001
46. Hyer HC, Sweeney DC, Petrie CM (2022) Functional fiber-optic sensors embedded in stainless steel components using ultrasonic additive manufacturing for distributed temperature and strain measurements. Addit Manuf 52:102681. https://doi.org/10.1016/j.addma.2022.102681
47. Chilelli SK, Schomer JJ, Dapino MJ (2019) Detection of crack initiation and growth using fiber Bragg grating sensors embedded into metal structures through ultrasonic additive manufacturing. Sensors 19:4917. https://doi.org/10.3390/s19224917
48. C Petrie, N Niyanth S, C Frederick, T Mcfalls, S Babu, A Hehr, M Norfolk, J Sheridan (2019) Embedded Fiber-Optic Sensors for In-Pile Applications, Oak Ridge National Laboratory (ORNL), Oak Ridge, TN (United States). https://www.osti.gov/biblio/1526394 (accessed October 10, 2024).
49. Bournias-Varotsis A, Han X, Harris RA, Engstrøm DS (2019) Ultrasonic additive manufacturing using feedstock with build-in circuitry for 3D metal embedded electronics. Addit Manuf 29:100799. https://doi.org/10.1016/j.addma.2019.100799
50. Petrie CM, Sridharan N, Subramanian M, Hehr A, Norfolk M, Sheridan J (2019) Embedded metallized optical fibers for high temperature applications*. Smart Mater Struct 28:055012. https://doi.org/10.1088/1361-665X/ab0b4e
51. Bournias-Varotsis A, Friel RJ, Harris RA, Engstrøm DS (2018) Ultrasonic additive manufacturing as a form-then-bond process for embedding electronic circuitry into a metal matrix. J Manuf Process 32:664–675. https://doi.org/10.1016/j.jmapro.2018.03.027
52. Monaghan T, Capel AJ, Christie SD, Harris RA, Friel RJ (2015) Solid-state additive manufacturing for metallized optical fiber integration. Compos Part A Appl Sci Manuf 76:181–193. https://doi.org/10.1016/j.compositesa.2015.05.032

53. Moreno-Gomez A, Perez-Ramirez CA, Dominguez-Gonzalez A, Valtierra-Rodriguez M, Chavez-Alegria O, Amezquita-Sanchez JP (2018) Sensors used in structural health monitoring. Arch Comput Methods Eng 25:901–918. https://doi.org/10.1007/s11831-017-9217-4
54. 1347065903.pdf, (n.d.). https://www.aschome.com/administrator/images/support/pdf/1347065903.pdf (accessed November 10, 2024).
55. What is a type K Thermocouple?, Httpswwwomegacomen-Us (n.d.). https://www.omega.com/en-us/resources/k-type-thermocouples (accessed November 10, 2024).
56. Type J Thermocouple, (n.d.). https://tempsens.com/blog/type-j-thermocouple (accessed November 10, 2024).
57. Type T Thermocouple - Leading Manufacturer of Thermocouples | TC Inc., (n.d.). https://www.tc-inc.com/thermocouples/type-t-thermocouple.html (accessed November 10, 2024).
58. Inyushkin AV, Leicht K, Esquinazi P (1998) Magnetic field dependence of the sensitivity of a type E (chromel–constantan) thermocouple. Cryogenics 38:299–304. https://doi.org/10.1016/S0011-2275(97)00156-2
59. Burley NA (1990) Advanced integrally sheathed type N thermocouple of ultra-high thermoelectric stability. Measurement 8:36–41. https://doi.org/10.1016/0263-2241(90)90075-H
60. Resistance thermometer, Wikipedia (2024). https://en.wikipedia.org/w/index.php?title=Resistance_thermometer&oldid=1262250676 (accessed January 19, 2025).
61. Jiang X, Kim K, Zhang S, Johnson J, Salazar G (2014) High-temperature piezoelectric sensing. Sensors 14:144–169. https://doi.org/10.3390/s140100144
62. Zhgoon SA, Shvetsov AS, Sakharov SA, Elmazria O (2018) High-temperature SAW resonator sensors: electrode design specifics. IEEE Trans Ultrason Ferroelectr Freq Control 65:657–664. https://doi.org/10.1109/TUFFC.2018.2797093
63. Fibre Bragg Grating Sensor - an overview | ScienceDirect Topics, (n.d.). https://www.sciencedirect.com/topics/engineering/fibre-bragg-grating-sensor (accessed January 19, 2025).
64. S. Lomperski, C. Gerardi, D. Lisowski, Fiber Optic Distributed Sensors for High-resolution Temperature Field Mapping, J. Vis. Exp. JoVE (2016) 54076. https://doi.org/10.3791/54076.
65. Lindner M, Stadler A, Hamann G, Fischer B, Jakobi M, Heilmeier F, Bauer C, Volk W, Koch AW, Roths J (2021) Fiber Bragg sensors embedded in cast aluminum parts: axial strain and temperature response. Sensors 21:1680. https://doi.org/10.3390/s21051680
66. P Robert, N Béraud, M Museau, H Paris 2021 A guide to select strain sensors to be embedded in smart metal parts built by WAAM, in: Conférence Manuf. 21, Angers (Virtuel), France. https://hal.science/hal-03350560 (accessed January 19, 2025).
67. Strain Gauge, Httpswwwomegacomen-Us (n.d.). https://www.omega.com/en-us/resources/strain-microstrain (accessed January 19, 2025).
68. K. Hoffmann, An Introduction to Stress Analysis and Transducer Design using Strain Gauges, (n.d.).
69. C. Ruiz, Strain Gauges, in: Thermopedia, Begel House Inc., 2011. https://doi.org/10.1615/AtoZ.s.strain_gauges.
70. High Temperature | Micro-Measurements, (n.d.). https://www.micro-measurements.com/high-temperature (accessed December 6, 2024).
71. High-Temperature-Thin-Film-Strain-Gauges.pdf, (n.d.). https://www1.grc.nasa.gov/wp-content/uploads/High-Temperature-Thin-Film-Strain-Gauges.pdf (accessed January 19, 2025).
72. Chen J, Liu B, Zhang H (2011) Review of fiber Bragg grating sensor technology. Front Optoelectron China 4:204–212. https://doi.org/10.1007/s12200-011-0130-4
73. Bhaskar CVN, Pal S, Pattnaik PK (2021) Recent advancements in fiber Bragg gratings based temperature and strain measurement. Results Opt 5:100130. https://doi.org/10.1016/j.rio.2021.100130
74. Mandal D, Banerjee S (2022) Surface Acoustic Wave (SAW) sensors: physics, materials, and applications. Sensors 22:820. https://doi.org/10.3390/s22030820
75. Laurent ML, Marquis GE, Gonzalez M, Tansel I, Tosunoglu S (2025) Embedded sensing in additive manufacturing metal and polymer parts: a comparative study of integration techniques and structural health monitoring performance. Algorithms 18:613. https://doi.org/10.3390/a18100613
76. How Piezoelectric Sensors Work? - APC International, (n.d.). https://www.americanpiezo.com/blog/how-piezoelectric-sensors-work/ (accessed January 19, 2025).
77. Ju M, Dou Z, Li J-W, Qiu X, Shen B, Zhang D, Yao F-Z, Gong W, Wang K (2023) Piezoelectric materials and sensors for structural health monitoring: fundamental aspects, current status, and future perspectives. Sensors 23:543. https://doi.org/10.3390/s23010543
78. Comparison of BSPT and PZT Piezoelectric Ceramic Transformers for High-Temperature Power Supplies - Forrester - 2022 - Advanced Engineering Materials - Wiley Online Library, (n.d.). https://advanced.onlinelibrary.wiley.com/doi/full/https://doi.org/10.1002/adem.202200513 (accessed November 11, 2025).
79. Zhu L, Fu Y, Chow R, Spencer BF, Park JW, Mechitov K (2018) Development of a high-sensitivity wireless accelerometer for structural health monitoring. Sensors 18:262. https://doi.org/10.3390/s18010262
80. Wang J, Tang X, Gao RX, Duan L, Zhang L (2016) On ultrasonic communication through metal structure for machine embedded sensing. Measurement 94:653–662. https://doi.org/10.1016/j.measurement.2016.09.015
81. Kazanskiy NL, Khonina SN, Butt MA (2022) Advancement in Silicon Integrated Photonics Technologies for sensing applications in near-infrared and mid-infrared region: a review. Photonics 9:331. https://doi.org/10.3390/photonics9050331
82. K.R. Brinker, Passively-Coded Embedded Microwave Sensors for Materials Characterization and Structural Health Monitoring (SHM), M.S.E.E., Missouri University of Science and Technology, 2019. https://www.proquest.com/docview/2303836578/abstract/55417BDDCB0842F0PQ/1 (accessed October 26, 2024).
83. Ferreira PM, Caçador D, Machado MA, Carvalho MS, Vilaça P, Sorger G, Farias FWC, Figueiredo AR, Vidal C (2024) Enabling electrical response through piezoelectric particle integration in AA2017-T451 aluminium parts using FSP technology. Smart Mater Struct 33:065037. https://doi.org/10.1088/1361-665X/ad4d45
84. Ferreira PM, Caçador D, Machado MA, Carvalho MS, Vilaça P, Sorger G, Farias FWC, Figueiredo AR, Vidal C (2025) Smart piezoelectric composite: impact of piezoelectric ceramic microparticles embedded in heat-treated 7075–T651 aluminium alloy. Int J Mech Mater Des 21:155–180. https://doi.org/10.1007/s10999-024-09731-7
85. R Hahnlen, MJ Dapino (2010) Active metal-matrix composites with embedded smart materials by ultrasonic additive manufacturing, in: Ind. Commer. Appl. Smart Struct. Technol. SPIE, 2010: pp. 159–170. https://doi.org/10.1117/12.848853.
86. Stoll P, Gasparin E, Spierings A, Wegener K (2021) Embedding eddy current sensors into LPBF components for structural health monitoring. Prog Addit Manuf 6:445–453. https://doi.org/10.1007/s40964-021-00204-3
87. Wang W, Zong R, Li D, Zhang J, Teng G, Li S (2025) High-temperature strain gauge measurement techniques for temperatures above 800 °C: a review. Materials 18:1588. https://doi.org/10.3390/ma18071588
88. Ren F, Giannakeas IN, Sharif Khodaei Z, Aliabadi MHF (2024) The temperature effects on embedded PZT signals in structural

health monitoring for composite structures with different thicknesses. NDT E Int 141:102988. https://doi.org/10.1016/j.ndteint.2023.102988
89. Guimarães B, Fernandes CM, Figueiredo D, Carvalho O, Miranda G, Silva FS (2024) Multi-material laser powder bed fusion of embedded thermocouples in WC-Co cutting tools. J Manuf Process 118:163–172. https://doi.org/10.1016/j.jmapro.2024.03.025
90. Zhang Z, Liu Z, Lei J, Chen L, Li L, Zhao N, Fang X, Ruan Y, Tian B, Zhao L (2023) Flexible thin film thermocouples: from structure, material, fabrication to application. iScience 26:107303. https://doi.org/10.1016/j.isci.2023.107303
91. Díez-Sierra J, Martínez A, Etxarri I, Azpitarte I, Pozo B, Quintana I (2022) Manufacturing smart surfaces with embedded sensors via magnetron sputtering and laser scribing. Appl Surf Sci 606:154844. https://doi.org/10.1016/j.apsusc.2022.154844
92. Review of Wireless RFID Strain Sensing Technology in Structural Health Monitoring, (n.d.). https://www.mdpi.com/1424-8220/23/15/6925 (accessed November 6, 2025).
93. High-Sensitivity RFID Sensor for Structural Health Monitoring - Nesser - 2023 - Advanced Science - Wiley Online Library, (n.d.). https://advanced.onlinelibrary.wiley.com/doi/https://doi.org/10.1002/advs.202301807 (accessed November 6, 2025).
94. J.J. Schomer, A.J. Hehr, M.J. Dapino, Characterization of embedded fiber optic strain sensors into metallic structures via ultrasonic additive manufacturing, in: J.P. Lynch (Ed.), Las Vegas, Nevada, United States, 2016: p. 980320. https://doi.org/10.1117/12.2219690.
95. Pan X, Lin F, Wu C, Zeng Y, Chen G, Chen Q, Sun D, Hai Z (2022) Additive-manufactured platinum thin-film strain gauges for structural microstrain testing at elevated temperatures. Micromachines 13:1472. https://doi.org/10.3390/mi13091472
96. AR Marotta (2019) Printable Thin-Film Sol-Gel Lead Zirconate Titanate (PZT) Deposition Using NanoJet and Inkjet Printing Methods, M.S., Rochester Institute of Technology. https://www.proquest.com/docview/2301893601/abstract/9D3B369FBCDE4B9CPQ/1 (accessed January 20, 2025).
97. FN Mullaveettil (2022) Additive manufacturing and experimental research of polyvinylidene fluoride cellular structures and transducers /, Kauno technologijos universitetas. https://epubl.ktu.edu/object/elaba:118320868/ (accessed January 20, 2025).
98. Linden J, Melech N, Sakaev I, Fogel O, Krylov S, Nuttman D, Zalevsky Z, Sirota M (2023) Femtosecond laser-assisted fabrication of piezoelectrically actuated crystalline quartz-based MEMS resonators. Microsyst Nanoeng 9:38. https://doi.org/10.1038/s41378-023-00511-5
99. Zega V, Invernizzi M, Bernasconi R, Cuneo F, Langfelder G, Magagnin L, Levi M, Corigliano A (2019) The first 3D-printed and wet-metallized three-axis accelerometer with differential capacitive sensing. IEEE Sens J 19:9131–9138. https://doi.org/10.1109/JSEN.2019.2924473
100. Li Y, Guo S, Su Z, Ding K, Loh XJ (2025) Lightweight and conformal acousto-ultrasonic sensing network for multi-scale structural health monitoring: a review. FlexMat 2:4–29. https://doi.org/10.1002/flm2.35
101. Liu G, Xiong Y, Zhou L (2021) Additive manufacturing of continuous fiber reinforced polymer composites: design opportunities and novel applications. Compos Commun 27:100907. https://doi.org/10.1016/j.coco.2021.100907
102. M Zenou, L Grainger (2018) 3 - Additive manufacturing of metallic materials, in: J. Zhang, Y.-G. Jung (Eds.), Addit. Manuf., Butterworth-Heinemann. pp. 53–103. https://doi.org/10.1016/B978-0-12-812155-9.00003-7.
103. Gaikwad A, Williams RJ, de Winton H, Bevans BD, Smoqi Z, Rao P, Hooper PA (2022) Multi phenomena melt pool sensor data fusion for enhanced process monitoring of laser powder bed fusion additive manufacturing. Mater Des 221:110919. https://doi.org/10.1016/j.matdes.2022.110919
104. Zeng C, Xue J, Jia Y, Luo S, Huang F, Liu X, Du Y (2024) A review of additive manufacturing of metallic materials assisted by electromagnetic field technology. J Manuf Process 131:920–946. https://doi.org/10.1016/j.jmapro.2024.09.078
105. Mishra AK, Kumar A (2019) Numerical and experimental analysis of the effect of volumetric energy absorption in powder layer on thermal-fluidic transport in selective laser melting of Ti6Al4V. Opt Laser Technol 111:227–239. https://doi.org/10.1016/j.optlastec.2018.09.054
106. Li JN, Gong SL, Liu KG, Qi WJ, Tian J, Shan FH (2019) Formation mechanism and mechanical properties of the selective laser melting Ni/Co base alloy. J Alloys Compd 777:963–967. https://doi.org/10.1016/j.jallcom.2018.10.343
107. Galbusera F, Caprio L, Previtali B, Demir AG (2023) The influence of novel beam shapes on melt pool shape and mechanical properties of LPBF produced Al-alloy. J Manuf Process 85:1024–1036. https://doi.org/10.1016/j.jmapro.2022.12.007
108. Gu D, Hagedorn Y-C, Meiners W, Meng G, Batista RJS, Wissenbach K, Poprawe R (2012) Densification behavior, microstructure evolution, and wear performance of selective laser melting processed commercially pure titanium. Acta Mater 60:3849–3860. https://doi.org/10.1016/j.actamat.2012.04.006
109. Yi JH, Kang JW, Wang TJ, Wang X, Hu YY, Feng T, Feng YL, Wu PY (2019) Effect of laser energy density on the microstructure, mechanical properties, and deformation of Inconel 718 samples fabricated by selective laser melting. J Alloys Compd 786:481–488. https://doi.org/10.1016/j.jallcom.2019.01.377
110. Kamath C, El-dasher B, Gallegos GF, King WE, Sisto A (2014) Density of additively-manufactured, 316L SS parts using laser powder-bed fusion at powers up to 400 W. Int J Adv Manuf Technol 74:65–78. https://doi.org/10.1007/s00170-014-5954-9
111. Gu DD, Meiners W, Wissenbach K, Poprawe R (2012) Laser additive manufacturing of metallic components: materials, processes and mechanisms. Int Mater Rev. https://doi.org/10.1179/1743280411Y.0000000014
112. Trevisan F, Calignano F, Lorusso M, Pakkanen J, Aversa A, Ambrosio EP, Lombardi M, Fino P, Manfredi D (2017) On the selective laser melting (SLM) of the AlSi10Mg alloy: process, microstructure, and mechanical properties. Materials 10:76. https://doi.org/10.3390/ma10010076
113. Pragana JPM, Sampaio RFV, Bragança IMF, Silva CMA, Martins PAF (2021) Hybrid metal additive manufacturing: a state–of–the-art review. Adv Ind Manuf Eng 2:100032. https://doi.org/10.1016/j.aime.2021.100032
114. Harun WSW, Kamariah MSIN, Muhamad N, Ghani SAC, Ahmad F, Mohamed Z (2018) A review of powder additive manufacturing processes for metallic biomaterials. Powder Technol 327:128–151. https://doi.org/10.1016/j.powtec.2017.12.058
115. Abedi M, Moskovskikh D, Romanovski V, Ozherelkov D, Gromov A (2024) Unlocking the potential of graphene-reinforced AlSi10Mg nanocomposites in laser powder bed fusion: a comprehensive review. J Alloys Compd 978:173441. https://doi.org/10.1016/j.jallcom.2024.173441
116. Cheng XY, Li SJ, Murr LE, Zhang ZB, Hao YL, Yang R, Medina F, Wicker RB (2012) Compression deformation behavior of Ti–6Al–4V alloy with cellular structures fabricated by electron beam melting. J Mech Behav Biomed Mater 16:153–162. https://doi.org/10.1016/j.jmbbm.2012.10.005
117. Qi X, Liang X, Wang J, Zhang H, Wang X, Liu Z (2024) Microstructure tailoring in laser powder bed fusion (L-PBF): strategies, challenges, and future outlooks. J Alloys Compd 970:172564. https://doi.org/10.1016/j.jallcom.2023.172564
118. ZainElabdeen IH, Ismail L, Mohamed OF, Khan KA, Schiffer A (2024) Recent advancements in hybrid additive manufacturing of

similar and dissimilar metals via laser powder bed fusion. Mater Sci Eng A 909:146833. https://doi.org/10.1016/j.msea.2024.146833
119. Gibson I, Rosen D, Stucker B, Khorasani M (2021) Additive Manufacturing Technologies. Springer, Cham
120. Mohammadhosseini A, Masood SH, Fraser D, Jahedi M (2015) Dynamic compressive behaviour of Ti-6Al-4V alloy processed by electron beam melting under high strain rate loading. Adv Manuf 3:232–243. https://doi.org/10.1007/s40436-015-0119-0
121. Alkhatib SE, Sercombe TB (2022) High strain-rate response of additively manufactured light metal alloys. Mater Des 217:110664. https://doi.org/10.1016/j.matdes.2022.110664
122. Zhou Q, Zhang XZ, Tang HP, Qian M (2023) Electron beam additively manufactured Ti–1Al–8V–5Fe alloy: in-situ precipitation hardening, tensile properties and fracture characteristics. Mater Sci Eng A 865:144639. https://doi.org/10.1016/j.msea.2023.144639
123. Liu N, Niu J, Chen Y, Wang X, Wang J, Xiang H, Wei D, Chen G (2023) Effect of in-situ post-heating on the microstructure and tensile performance of TiAl alloys produced via selective electron beam melting. Mater Sci Eng A 885:145585. https://doi.org/10.1016/j.msea.2023.145585
124. Li SJ, Murr LE, Cheng XY, Zhang ZB, Hao YL, Yang R, Medina F, Wicker RB (2012) Compression fatigue behavior of Ti–6Al–4V mesh arrays fabricated by electron beam melting. Acta Mater 60:793–802. https://doi.org/10.1016/j.actamat.2011.10.051
125. Rafi HK, Karthik NV, Gong H, Starr TL, Stucker BE (2013) Microstructures and mechanical properties of Ti6Al4V parts fabricated by selective laser melting and electron beam melting. J Mater Eng Perform 22:3872–3883. https://doi.org/10.1007/s11665-013-0658-0
126. HM Alojaly, A Hammouda, KY Benyounis (2024) 12.27 - Review of recent developments on metal matrix composites with particulate reinforcement, in: S. Hashmi (Ed.), Compr. Mater. Process. Second Ed., Elsevier, Oxford. pp. 350–373. https://doi.org/10.1016/B978-0-323-96020-5.00041-8.
127. Uçak N, Çiçek A, Aslantas K (2022) Machinability of 3D printed metallic materials fabricated by selective laser melting and electron beam melting: a review. J Manuf Process 80:414–457. https://doi.org/10.1016/j.jmapro.2022.06.023
128. Zhang L-C, Liu Y, Li S, Hao Y (2018) Additive manufacturing of titanium alloys by electron beam melting: a review. Adv Eng Mater 20:1700842. https://doi.org/10.1002/adem.201700842
129. Tammas-Williams S, Zhao H, Léonard F, Derguti F, Todd I, Prangnell PB (2015) XCT analysis of the influence of melt strategies on defect population in Ti–6Al–4V components manufactured by selective electron beam melting. Mater Charact 102:47–61. https://doi.org/10.1016/j.matchar.2015.02.008
130. Badoniya P, Srivastava M, Jain PK, Rathee S (2024) A state-of-the-art review on metal additive manufacturing: milestones, trends, challenges and perspectives. J Braz Soc Mech Sci Eng 46:339. https://doi.org/10.1007/s40430-024-04917-8
131. Dinda GP, Song L, Mazumder J (2008) Fabrication of Ti-6Al-4V scaffolds by direct metal deposition. Metall Mater Trans A 39:2914–2922. https://doi.org/10.1007/s11661-008-9634-y
132. Song L, Bagavath-Singh V, Dutta B, Mazumder J (2012) Control of melt pool temperature and deposition height during direct metal deposition process. Int J Adv Manuf Technol 58:247–256. https://doi.org/10.1007/s00170-011-3395-2
133. Freeman FSHB, Thomas B, Chechik L, Todd I (2022) Multi-faceted monitoring of powder flow rate variability in directed energy deposition. Addit Manuf Lett 2:100024. https://doi.org/10.1016/j.addlet.2021.100024
134. Imran MM, Che Idris A, De Silva LC, Kim Y-B, Abas PE (2024) Advancements in 3D printing: directed energy deposition techniques, defect analysis, and quality monitoring. Technologies 12:86. https://doi.org/10.3390/technologies12060086
135. Ji W, Zhou R, Viveganandhan P, See Wu M, Gao H, Zhou K (2023) Recent progress in gradient-structured metals and alloys. Prog Mater Sci 140:101194. https://doi.org/10.1016/j.pmatsci.2023.101194
136. Piscopo G, Iuliano L (2022) Current research and industrial application of laser powder directed energy deposition. Int J Adv Manuf Technol 119:6893–6917. https://doi.org/10.1007/s00170-021-08596-w
137. Svetlizky D, Zheng B, Vyatskikh A, Das M, Bose S, Bandyopadhyay A, Schoenung JM, Lavernia EJ, Eliaz N (2022) Laser-based directed energy deposition (DED-LB) of advanced materials. Mater Sci Eng A 840:142967. https://doi.org/10.1016/j.msea.2022.142967
138. Mo B, Li T, Deng L, Shi F, Liu W, Zhang H (2024) Mechanisms and influencing factors of defect formations during laser-based directed energy deposition with coaxial powder feeding: a review. Virtual Phys Prototyp 19:e2404155. https://doi.org/10.1080/17452759.2024.2404155
139. Farias FWC, dos Santos TJG, Oliveira JP (2024) Directed energy deposition+mechanical interlayer deformation additive manufacturing: a state-of-the-art literature review. Int J Adv Manuf Technol 131:999–1038. https://doi.org/10.1007/s00170-024-13126-5
140. Piscopo G, Atzeni E, Saboori A, Salmi A (2023) An overview of the process mechanisms in the laser powder directed energy deposition. Appl Sci 13:117. https://doi.org/10.3390/app13010117
141. EM Palmero, A Bollero (2021) 3D and 4D Printing of Functional and Smart Composite Materials, In: D Brabazon (Ed.) Encycl Mater Compos, Elsevier, Oxford. pp. 402–419. https://doi.org/10.1016/B978-0-12-819724-0.00008-2.
142. Alagha AN, Hussain S, Zaki W (2021) Additive manufacturing of shape memory alloys: a review with emphasis on powder bed systems. Mater Des 204:109654. https://doi.org/10.1016/j.matdes.2021.109654
143. Lambiase F, Yanala PB, Pace F, Andreucci E, Paoletti A (2025) A state of the art review of wire arc additive manufacturing (WAAM)–part 1: process fundamentals, parameters and materials. Int J Adv Manuf Technol 138:4965–4993. https://doi.org/10.1007/s00170-025-15781-8
144. Habib N, Vafadar A, Guzzomi F (2025) A comparative study of aluminium properties manufactured using additive friction stir deposition (AFSD) and wire arc additive manufacturing (WAAM). Prog Addit Manuf 10:8963–8983. https://doi.org/10.1007/s40964-025-01217-y
145. Jadhav S, Kusekar S, Belure A, Digole S, Mali A, Cheepu M, Mugale M, Alkunte S, Kim D (2025) Recent progress and scientific challenges in wire-arc additive manufacturing of metallic multi-material structures. J Manuf Mater Process 9:284. https://doi.org/10.3390/jmmp9080284
146. Pagan M, Petrie C, Leonard D, Sridharan N, Zinkle S, Babu SS (2021) Interdiffusion of elements during ultrasonic additive manufacturing. Metall Mater Trans A 52:1142–1157. https://doi.org/10.1007/s11661-020-06131-2
147. RJ Friel (2015) 13 - Power ultrasonics for additive manufacturing and consolidating of materials, in: J.A. Gallego-Juárez, K.F. Graff (Eds.), Power Ultrason., Woodhead Publishing, Oxford. pp. 313–335. https://doi.org/10.1016/B978-1-78242-028-6.00013-2.
148. Richter B, Hocker SJA, Frankforter EL, Tayon WA, Glaessgen EH (2024) Influence of ultrasonic excitation on the melt pool and microstructure characteristics of Ti-6Al-4V at powder bed fusion additive manufacturing solidification velocities. Addit Manuf 89:104228. https://doi.org/10.1016/j.addma.2024.104228

149. Wang B, Yang F, Zhang H, He P (2023) Microstructure and interface evolution of diamond/Cu composites prepared via ultrasonic additive manufacturing (UAM). J Mater Res Technol 25:546–551. https://doi.org/10.1016/j.jmrt.2023.05.191
150. Wang B, Zhang H, Gao C, Lv W (2023) Microstructure and mechanical properties of Ti/Al laminates fabricated by ultrasonic additive manufacturing assisted by Joule heat and post-welding heat treatment. J Mater Res Technol 27:2149–2165. https://doi.org/10.1016/j.jmrt.2023.09.277
151. Gujba AK, Medraj M (2020) Power ultrasonic additive manufacturing: process parameters, microstructure, and mechanical properties. Adv Mater Sci Eng 2020:1064870. https://doi.org/10.1155/2020/1064870
152. Dehoff RR, Babu SS (2010) Characterization of interfacial microstructures in 3003 aluminum alloy blocks fabricated by ultrasonic additive manufacturing. Acta Mater 58:4305–4315. https://doi.org/10.1016/j.actamat.2010.03.006
153. N Sridharan, RR Dehoff, BH Jordan, SS Babu (2016) Development of coatings for ultrasonic additive manufacturing sonotrode using laser direct metal deposition process, Oak Ridge National Lab. (ORNL), Oak Ridge, TN (United States). https://doi.org/10.2172/1331097.
154. Behvar A, Shakil SI, Pirgazi H, Norfolk M, Haghshenas M (2024) Multi-layer solid-state ultrasonic additive manufacturing of aluminum/copper: local properties and texture. Int J Adv Manuf Technol 132:2061–2075. https://doi.org/10.1007/s00170-024-13490-2
155. Kong CY, Soar RC, Dickens PM (2004) Optimum process parameters for ultrasonic consolidation of 3003 aluminium. J Mater Process Technol 146:181–187. https://doi.org/10.1016/j.jmatprotec.2003.10.016
156. Li J, Monaghan T, Masurtschak S, Bournias-Varotsis A, Friel RJ, Harris RA (2015) Exploring the mechanical strength of additively manufactured metal structures with embedded electrical materials. Mater Sci Eng A 639:474–481. https://doi.org/10.1016/j.msea.2015.05.019
157. Zhang C, Yu H, Sun D, Liu W (2022) Ultrasonic additive manufacturing of metallic materials. Metals 12:1912. https://doi.org/10.3390/met12111912
158. Ozkan E (2024) Mechanical shock test simulation analysis of butterfly valves developed for the naval defense industry and evaluation of real test and production data. Sci Rep 14:9692. https://doi.org/10.1038/s41598-024-60302-4
159. Baraiya R, Babbar A, Jain V, Gupta D (2020) In-situ simultaneous surface finishing using abrasive flow machining via novel fixture. J Manuf Process 50:266–278. https://doi.org/10.1016/j.jmapro.2019.12.051
160. Hodgir R, Singh RK, Mujumdar S (2025) Strengthening of additively manufactured SS316L by in-situ laser remelting. Manuf Lett 44:942–947. https://doi.org/10.1016/j.mfglet.2025.06.111
161. Ye L, Xue H, Li Z, Zhou Y, Chen G, Xu F, Melentiev R, Newman S, Yu N (2025) Review of online quality control for laser directed energy deposition (LDED) additive manufacturing. Int J Extreme Manuf 7:062005. https://doi.org/10.1088/2631-7990/aded4f
162. van Blitterswijk RH, Botelho LA, Khajepour A (2025) Real-time multivariable control of directed energy deposition via adaptive model predictive control. Addit Manuf 111:104941. https://doi.org/10.1016/j.addma.2025.104941
163. Tang P, Zhao X, Shi H, Hu B, Ding J, Yang B, Xu W (2024) A review of multi-axis additive manufacturing: potential, opportunity and challenge. Addit Manuf 83:104075. https://doi.org/10.1016/j.addma.2024.104075
164. L Heinrich, J Fletcher, T Feldhausen, T Kurfess, C Saldaña (2022) Impact of Nozzle Condition on Powder Catchment Efficiency for Coaxial Powder Direct Energy Deposition. https://hdl.handle.net/2152/117334 (accessed October 10, 2024).
165. Lu C-L, He H, Ren J, Dhar J, Saunders G, Julius A, Samuel J, Wen JT (2025) Multi-robot scan-n-print for wire arc additive manufacturing. ASME Lett Transl Robotics. https://doi.org/10.1115/1.4067825
166. Omiyale BO, Ogedengbe II, Ogbeyemi A, Olugbade TO, Zhang WC, Farayibi PK (2025) Influence of heat input and uniform temperature distribution during wire arc additive manufacturing process: a critical review. Int J Adv Manuf Technol 138:2673–2695. https://doi.org/10.1007/s00170-025-15690-w
167. Dekis M, Tawfik M, Egiza M, Dewidar M (2025) Challenges and developments in wire arc additive manufacturing of steel: a review. Results Eng 26:104657. https://doi.org/10.1016/j.rineng.2025.104657
168. Guo C, Lin Q, Hu R, Wu S (2025) Research progress and application scenarios of wire + arc additive manufacturing: from process control to performance evaluation. Micromachines 16:749. https://doi.org/10.3390/mi16070749
169. Nazir A, Gokcekaya O, Md Masum Billah K, Ertugrul O, Jiang J, Sun J, Hussain S (2023) Multi-material additive manufacturing: a systematic review of design, properties, applications, challenges, and 3D printing of materials and cellular metamaterials. Mater Des 226:111661. https://doi.org/10.1016/j.matdes.2023.111661
170. Fathollahi S, Janssen PHM, Bekaert B, Vanderroost D, Vanhoorne V, Dickhoff BHJ (2024) Understanding powder behavior in continuous feeding: powder densification and screw layering. Powders 3:482–499. https://doi.org/10.3390/powders3040026
171. Kang X, Li G, Jiang W, Li F, Wang Y, Wang X, Zeng Q, Fan X (2025) Wire-based additive manufacturing of multi-material structures: a review. J Compos Sci 9:534. https://doi.org/10.3390/jcs9100534
172. Akin S, Chang T, Abir SSH, Kim YW, Xu S, Lim J, Sim Y, Lee J, Tsai J-T, Nath C, Lee H, Wu W, Samuel J, Lee CH, Jun MB-G (2024) One-step fabrication of functionalized electrodes on 3D-printed polymers for triboelectric nanogenerators. Nano Energy 129:110082. https://doi.org/10.1016/j.nanoen.2024.110082
173. YW Kim, S Akin, MB-G Jun, JW Sutherland, Cold Spray-Produced Functional Surfaces for Triboelectric Nanogenerators, in: n.d. https://doi.org/10.1115/IMECE2024-145320.
174. Kim YW, Akin S, Yun H, Xu S, Wu W, Jun MB-G (2022) Enhanced performance of triboelectric nanogenerators and sensors via cold spray particle deposition. ACS Appl Mater Interfaces 14:46410–46420. https://doi.org/10.1021/acsami.2c09367
175. Ameri B, Taheri-Behrooz F (2023) Advanced additive manufacturing of self-healing composites: exploiting shape memory alloys for autonomous restoration under mixed-mode loading. Mater Des 234:112379. https://doi.org/10.1016/j.matdes.2023.112379
176. Macías-Escrivá FD, Haber R, del Toro R, Hernandez V (2013) Self-adaptive systems: a survey of current approaches, research challenges and applications. Expert Syst Appl 40:7267–7279. https://doi.org/10.1016/j.eswa.2013.07.033
177. Soori M, Arezoo B (2025) Smart materials and alloys for additive manufacturing integration: a review. Addit Manuf Front 4:200242. https://doi.org/10.1016/j.amf.2025.200242
178. Abd-Elaziem W, Elkatatny S, Sebaey TA, Darwish MA, Abd El-Baky MA, hamada A (2024) Machine learning for advancing laser powder bed fusion of stainless steel. J Mater Res Technol 30:4986–5016. https://doi.org/10.1016/j.jmrt.2024.04.130
179. Huang DJ, Li H (2021) A machine learning guided investigation of quality repeatability in metal laser powder bed fusion additive manufacturing. Mater Des 203:109606. https://doi.org/10.1016/j.matdes.2021.109606
180. Gunasegaram DR, Barnard AS, Matthews MJ, Jared BH, Andreaco AM, Bartsch K, Murphy AB (2024) Machine learning-assisted in-situ adaptive strategies for the control of defects

and anomalies in metal additive manufacturing. Addit Manuf 81:104013. https://doi.org/10.1016/j.addma.2024.104013
181. Schena L, Marques PA, Poletti R, Ahizi S, den Van Berghe J, Mendez MA (2024) Reinforcement twinning: from digital twins to model-based reinforcement learning. J Comput Sci 82:102421. https://doi.org/10.1016/j.jocs.2024.102421

Terms and Conditions

Springer Nature journal content, brought to you courtesy of Springer Nature Customer Service Center GmbH (“Springer Nature”).
Springer Nature supports a reasonable amount of sharing of research papers by authors, subscribers and authorised users (“Users”), for small-scale personal, non-commercial use provided that all copyright, trade and service marks and other proprietary notices are maintained. By accessing, sharing, receiving or otherwise using the Springer Nature journal content you agree to these terms of use (“Terms”). For these purposes, Springer Nature considers academic use (by researchers and students) to be non-commercial.
These Terms are supplementary and will apply in addition to any applicable website terms and conditions, a relevant site licence or a personal subscription. These Terms will prevail over any conflict or ambiguity with regards to the relevant terms, a site licence or a personal subscription (to the extent of the conflict or ambiguity only). For Creative Commons-licensed articles, the terms of the Creative Commons license used will apply.
We collect and use personal data to provide access to the Springer Nature journal content. We may also use these personal data internally within ResearchGate and Springer Nature and as agreed share it, in an anonymised way, for purposes of tracking, analysis and reporting. We will not otherwise disclose your personal data outside the ResearchGate or the Springer Nature group of companies unless we have your permission as detailed in the Privacy Policy.
While Users may use the Springer Nature journal content for small scale, personal non-commercial use, it is important to note that Users may not:

1. use such content for the purpose of providing other users with access on a regular or large scale basis or as a means to circumvent access control;
2. use such content where to do so would be considered a criminal or statutory offence in any jurisdiction, or gives rise to civil liability, or is otherwise unlawful;
3. falsely or misleadingly imply or suggest endorsement, approval , sponsorship, or association unless explicitly agreed to by Springer Nature in writing;
4. use bots or other automated methods to access the content or redirect messages
5. override any security feature or exclusionary protocol; or
6. share the content in order to create substitute for Springer Nature products or services or a systematic database of Springer Nature journal content.

In line with the restriction against commercial use, Springer Nature does not permit the creation of a product or service that creates revenue, royalties, rent or income from our content or its inclusion as part of a paid for service or for other commercial gain. Springer Nature journal content cannot be used for inter-library loans and librarians may not upload Springer Nature journal content on a large scale into their, or any other, institutional repository.
These terms of use are reviewed regularly and may be amended at any time. Springer Nature is not obligated to publish any information or content on this website and may remove it or features or functionality at our sole discretion, at any time with or without notice. Springer Nature may revoke this licence to you at any time and remove access to any copies of the Springer Nature journal content which have been saved.
To the fullest extent permitted by law, Springer Nature makes no warranties, representations or guarantees to Users, either express or implied with respect to the Springer nature journal content and all parties disclaim and waive any implied warranties or warranties imposed by law, including merchantability or fitness for any particular purpose.
Please note that these rights do not automatically extend to content, data or other material published by Springer Nature that may be licensed from third parties.
If you would like to use or distribute our Springer Nature journal content to a wider audience or on a regular basis or in any other manner not expressly permitted by these Terms, please contact Springer Nature at

onlineservice@springernature.com